Nat Hazards (2018) 93:849–884
https://doi.org/10.1007/s11069-018-3328-6

ORIGINAL PAPER

Impact of climate change on landslides frequency: the Esino river basin case study (Central Italy)

Lorenzo Sangelantoni[1,2] · Eleonora Gioia[2] · Fausto Marincioni[2]

Received: 14 November 2017 / Accepted: 20 April 2018 / Published online: 27 April 2018

Abstract Researchers have long attempted to determine the amount of rainfall needed to trigger slope failures, yet relatively little progress has been reported on the effects of climate change on landslide initiation. Indeed, some relationships between landslides and climate change have been highlighted, but sign and magnitude of this correlation remain uncertain and influenced by the spatial and temporal horizon considered. This work makes use of statistically adjusted high-resolution regional climate model simulations, to study the expected changes of landslides frequency in the eastern Esino river basin (Central Italy). Simulated rainfall was used in comparison with rainfall thresholds for landslide occurrence derived by two observation-based statistical models (1) the cumulative event rainfall–rainfall duration model, and (2) the Bayesian probabilistic model. Results show an overall increase in projected landslide occurrence over the twenty-first century. This is especially confirmed in the high-emission scenario representative concentration pathway 8.5, where according to the first model, the events above rainfall thresholds frequency shift from ~ 0.025 to ~ 0.05 in the mountainous sector of the study area. Moreover, Bayesian analysis revealed the possible occurrence of landslide-triggering rainfall with a magnitude never occurred over the historical period. Landslides frequency change signal presents also considerable seasonal patterns, with summer displaying the steepest positive trend coupled to the highest inter-model spread. The methodological chain here proposed aims at representing a flexible tool for future landslide-hazard assessment, applicable over different areas and time horizons (e.g., short-term climate projections or seasonal forecasts).

Electronic supplementary material The online version of this article (https://doi.org/10.1007/s11069-018-3328-6) contains supplementary material, which is available to authorized users.

✉ Lorenzo Sangelantoni
l.sangelantoni@univpm.it

[1] Department of Physical and Chemical Sciences, CETEMPS, Università dell'Aquila, 67100 L'Aquila, Italy

[2] Department of Life and Environmental Sciences, Università Politecnica delle Marche, 60131 Ancona, Italy

Keywords Regional climate models · Regional climate change impacts · Rainfall thresholds for landslide occurrence · Landslide statistical modeling · Climate simulations bias correction

1 Introduction

Over the next decades, societies will face massive environmental changes potentially able to substantially alter life styles and priorities (Lenton et al. 2008). Climate change will possibly be the major driver of such changes. However, if on the one hand the scientific community unequivocally recognized over these past decades the connection between the increase in greenhouse gases (GHGs) concentration and the increase in global temperature (Bindoff et al. 2013), on the other hand, changes in the rainfall patterns as a second-order effect of the increased temperature is connoted by higher uncertainty. Such reservations concern the magnitude and frequency of extreme events, how they will scale across the globe in response to the increase in temperature (Seneviratne et al. 2012; Scoccimarro et al. 2013; Drobinski et al. 2016). Notwithstanding these uncertainties, a broad consensus prevails on the acceleration of the hydrological cycle in a warmer atmosphere (Trenberth 1999; Mariotti et al. 2002; Lorenz and DeWeaver 2007; Volosciuk et al. 2016); acceleration appears strongly affected by the local-scale morphological and orographic peculiarities. (Xoplaki et al. 2004; Walsh et al. 2014).

Rainfall is a major trigger of landslides (e.g., De Vita and Reichenbach 1998; Guzzetti et al. 2007), one of the most widespread geohydrological hazards over the world, and an increase in rainfall frequency and intensity may directly affect landslides frequency and magnitude thus increasing ensuing damages and fatalities. Indeed, good progresses have been made in linking the amount of rainfall needed to trigger slope failures (e.g., Crozier 1996; Aleotti 2004; Guzzetti et al. 2007; Martinotti et al. 2017), yet the nexus between climate change and landslide initiation appears more complicated and requires further study (Dikau and Schrott 1999; McInnes et al. 2007; Crozier 2010; Coe and Godt 2012). The available literature indicates a relationship between landslides and climate change, but the sign and strength of this correlation remain uncertain and extremely influenced by the spatial and temporal horizon considered (Seneviratne et al. 2012; Gariano and Guzzetti 2016). Landslides, strictly depending on geological, geomorphological, and land cover contexts, represent a category of climate change-related impacts (Pisano et al. 2017), which understanding and management require specific considerations. Moreover, the implementation of effective landslide adaptation measures depends on the availability of plausible multi-scale information about future climate trends. Regional climate model (RCM) simulations are considered primary tools for climate impact studies focusing on rainfall and other key climate variables (Giorgi 1990; Giorgi and Mearns 1999; Giorgi et al. 2009; Hawkins and Sutton 2009; Jacob et al. 2014). However, even the newest generation of RCM is still affected by systematic errors that can deeply bias impact models results (Boberg and Christensen 2012). Such errors are mainly due to the imperfections on physical formulation and unpredictability of future natural variability (Christensen et al. 2008; Boberg and Christensen 2012; Bellprat et al. 2013; Casati et al. 2013). Furthermore, climate simulations are affected by the representativeness error arising not much from erroneous physical formulation, but rather from the spatial-scale mismatch between simulated and observed fields (Casati et al. 2013; Tomozeiu et al. 2013). The combination of these errors contributes to the different statistical properties shown by climate simulations and observations. For this reason, nowadays it is a standard procedure to post-process simulation outputs toward observations.

In this work, we model future trends of landslide occurrence on three representative sites (Ancona, Jesi, and Apiro) of the eastern Esino river basin, Marche Region, Central Italy. We connect simulated rainfall from three RCMs (EURO-CORDEX project, Jacob et al. 2014) to rainfall thresholds for landslide occurrence computed using two different statistical models. Our simulations are post-processed (i.e., statistically adjusted) through a quantile mapping (QM) technique necessary to map the statistical properties of the observations to the simulations (Boé et al. 2007; Themeßl et al. 2011b; Berg et al. 2012; Gudmundsson et al. 2012). However, because QM is also known for potentially altering the original climate change signal (CCS) produced by the climate models (Giorgi and Coppola 2010; Themeßl et al. 2011a; Maraun 2013; Gennaretti et al. 2015; Sangelantoni et al. 2018), we opted for the configuration proposed by Cannon et al. (2015), quantile delta mapping (QDM), which preserves the original CCS. Once post-processed, the simulated temporal evolution of rainfall is juxtaposed to the thresholds computed with two statistical landslide predictive models: (1) the cumulative event rainfall–rainfall duration (ED) model, and (2) the Bayesian probabilistic model. In Fig. 1, the entire methodological chain to define future changes in landslide occurrence frequency is summarized.

2 Study area and materials

2.1 Study area

Data collection was carried out in the eastward section of the Esino river catchment area (Fig. 2), one of the largest and most inhabited watersheds of the Marche Region in central Italy (National Institute of Statistics—ISTAT 2016). The high exposure to landslides of this urbanized area, besides making this study salient, provides for abound information of past events.

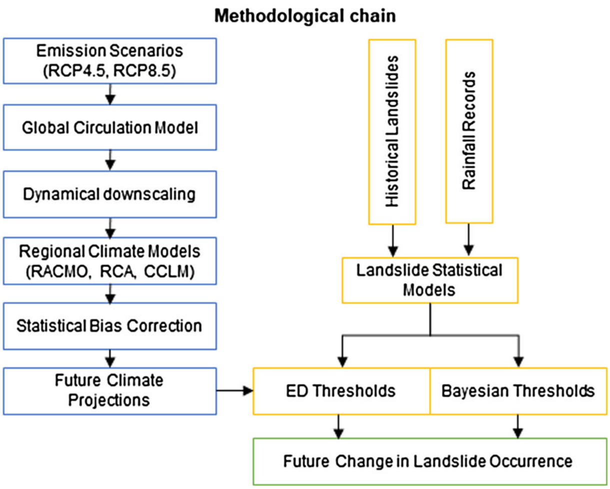

Fig. 1 Reference methodological framework for the definition of future changes in landslide occurrence. Modified after Gariano and Guzzetti (2016)

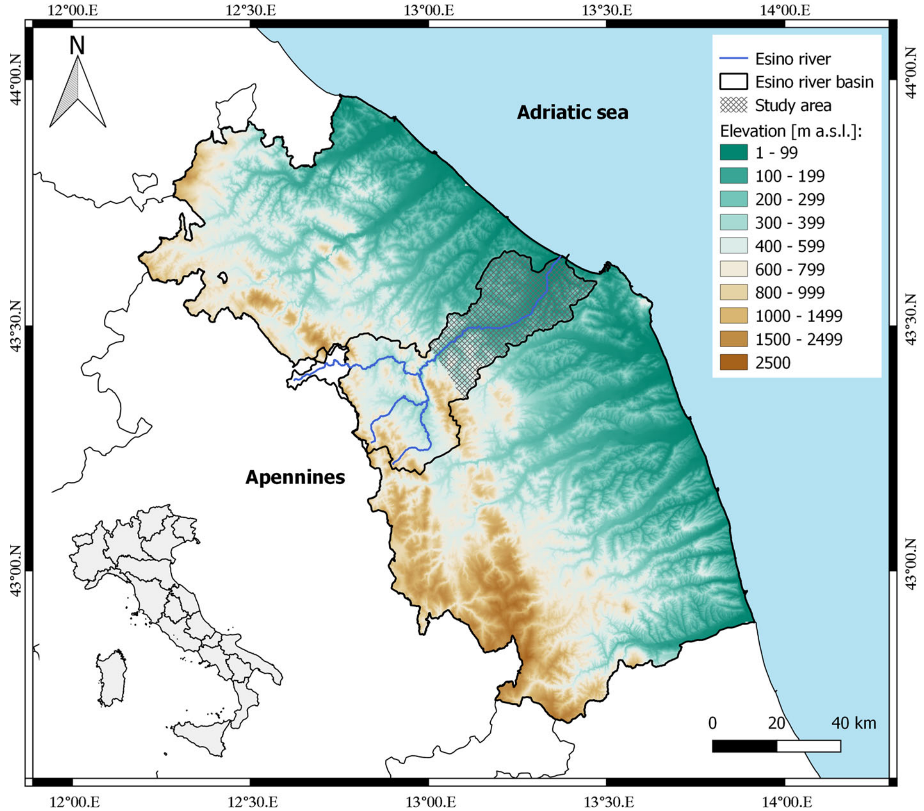

Fig. 2 Study area within the Esino river basin (Marche Region, Central Italy)

This study area covers about 550 km^2 and stretches from the Sub-Apennine hills on the West to the Adriatic coast on the East (Gentili and Dramis 1997). The outcrop, made of sedimentary sequences of mainly clay, silt, and sand (Fig. 3), is affected by numerous shallow landslides. These movements show great variability in size and type (flows and slides) and affect the transitional layer between the weathered material and the bedrock (Bisci and Dramis 1991; Cardinali and Guzzetti 2003).

The changing permeability of these terrains plays a very important role in determining the relationship between landslides and rainfall. Typically, the lithology of this area has medium–low permeability, allowing moderate rain storage and quick soil saturation. For this reason, landslide triggering is directly linked to the cumulative values (Peruccacci et al. 2012) as well as intensity and duration of rainfall (Gioia et al. 2015). Indeed, changes in the hydrological cycle connected to climate change will plausibly influence landslides initiation within this considered territory.

2.2 Landslides dataset

Based on the dataset of historical landslides provided by the Marche Region's Civil Protection Monitoring and Forecasting Center, the study area was affected by 208 rainfall-triggered landslides over the period 1990–2012 (Fig. 4). These records mainly consist of

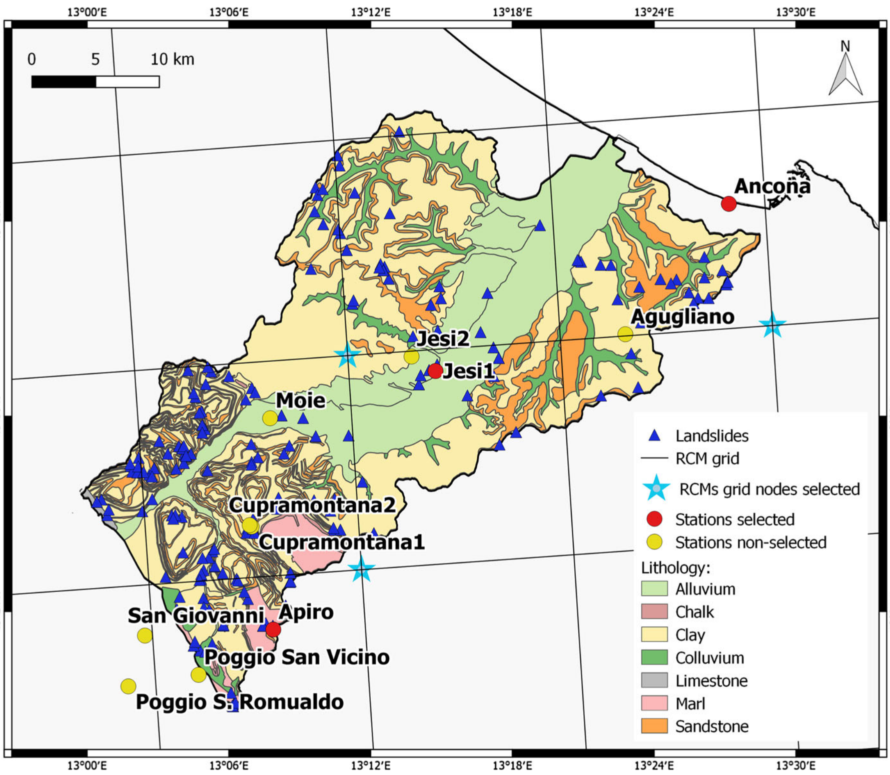

Fig. 3 Study area sediments divided by lithology. The circles (yellow and red) represent the rain gauge stations, while the triangles indicate the georeferenced landslides. Red circles denote the stations selected for providing rainfall observed time series. Finally, the figure shows a representative RCM grid with light blue stars indicating the nodes providing rainfall simulations

shallow landslides, usually with an average depth of 1 m, triggered near transportation infrastructures and civil or industrial buildings. Such landslides have been reported to the authorities and to the press mostly because of the damages caused or the media exposure reached on the territory. Therefore, the dataset may not be completely exhaustive of the actual instability conditions of the study area.

According to the lithological map by Folchi Vici D'Arcevia et al. (2008), almost all the landslides were triggered in clay (100) or sandstone (64) materials, in areas where the land use is generally agricultural (European Commission 2004). The remaining ones were activated in alluvium (25), marl (13), colluvium (3) and limestone (3) lithologies.

Using a criterion of proximity, each landslide has been attributed to a triggering rainfall deriving from the measurements of one of the 11 local weather stations, distributed in the study area or in the vicinity (Table 1 and Fig. 3). This dataset is provided by the Marche Region's Civil Protection Monitoring and Forecasting Center as well.

As a result, the 208 landslides have been related to 68 different rainfall events from December 1990 to May 2011 (Table 2 and Fig. 4). A rainfall event is here defined, with a standard procedure (Segoni et al. 2018), as a period of one or more days in which a continuing rainfall, with intensity $\geq$ 1 mm/day, is registered. Subsequently, two consecutive rainfall events are separated by periods of one or more days with no rainfall or with

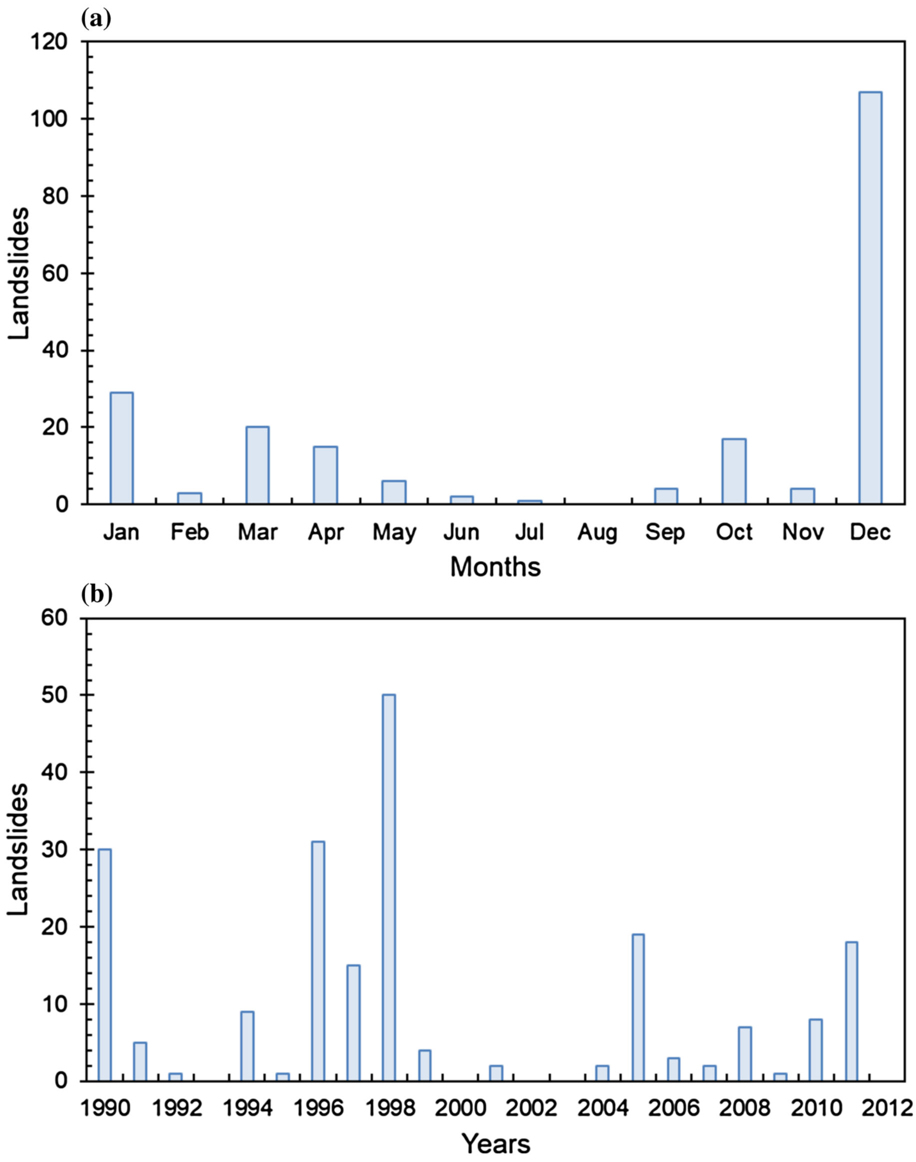

Fig. 4 Temporal distributions of the landslides triggered in the study area, per month (**a**) and per year (**b**) (1990–2012)

rainfall intensity < 1 mm/day. Each event initiated a certain number of landslides, from one to a maximum of 19. Table 2 gives an account of: (a) 5 rainfall events that triggered more than 10 landslides, (b) 16 rainfall events that triggered from 3 to 9 landslides, (c) 9 rainfall events that triggered 2 landslides, and (d) 38 rainfall events that triggered 1 landslide.

Table 1 List of the rain gauge stations available for the study area

Station	Station code	Data availability (years)	Elevation (m)
Agugliano	1220	2003-nowadays	170
Ancona	2009	1951-2014	6
Apiro	2066	1951-2009	516
Cupramontana 1	2062	1951-2008	506
Cupramontana 2	1263	2003-nowadays	510
Jesi 1	2063	1951-2008	96
Jesi 2	1213	2003-nowadays	100
Moie	2067	1951-2014	110
Poggio San Romualdo	2064	1991-2007	926
Poggio San Vicino	2848	2009-nowadays	580
Fabriano	1413	2001-nowadays	625

Highlighted are the stations selected as reference sites for this work

2.3 Rainfall datasets

For what concerns the climate analysis, we use two daily rainfall datasets: (1) observed rainfall, and (2) simulated rainfall.

The observed daily cumulative rainfall dataset covers the period 1971–2000, which is the temporal segment used as calibration period for the statistical adjustment of rainfall simulations. This dataset is provided by the Marche Region’s Civil Protection Monitoring and Forecasting Center. The quality of such database was checked according to “Guide to Climatological Data” (WMO 2007) as performed in Appiotti et al. (2014). Three rain gauges stations located in Ancona, Jesi 1—named “Jesi” hereafter—and Apiro (Table 1) have been chosen to represent the three main climate sectors of the eastward section of the Esino river catchment area, which includes a hilly mountainous area to the West (the Apennines range) and a coastal area to the East (the Adriatic seaboard) (Fig. 2). Furthermore, these three stations provide the most complete and long observed datasets among those reported in Table 1. We refer to Ancona as the coast site, Jesi as the hill site, and Apiro as the mountain site.

The simulated daily cumulative rainfall dataset covers the period 1971–2099, which is the temporal segment provided by the three RCMs run (Table 3). These three RCMs represent a subset of the high-resolution RCM ensemble participating to the EURO-CORDEX initiative (Jacob et al. 2014) within the WRCP Coordinated Regional Downscaling Experiment (CORDEX, http://www.cordex.org/; Giorgi et al. 2009). A detailed description of the key features of the three RCMs considered in terms of grid configuration, physical schemes, and model performance can be found in the references reported in Table 3.

The simulated rainfall has been extracted from the grid point closest to the above-mentioned stations of Ancona, Jesi, and Apiro. Figure 3 reports the grid cells (for one representative RCM) distribution over the study area.

Simulations are forced by two different scenarios of atmospheric GHGs concentration, the representative concentration pathways (RCP) 4.5 and 8.5 (Moss et al. 2010; Meinshausen et al. 2011; Riahi et al. 2011). These two RCPs have been chosen as representative of a wider set of multi-gas emission scenarios (Meinshausen et al. 2011) and provide two

Table 2 List of the rainfall events that triggered one or more landslides within the study area during the period 1990–2012

Rainfall event (ID)	Station	Landslides	*D* (days)	*E* (mm)
Dec-90	Ancona	3	6	46.2
	Jesi 1	8	6	88.0
	Moie	19	6	54.8
Sep-91	Jesi 1	1	3	13.6
Nov-91	Ancona	1	3	61.6
	Apiro	1	3	87.4
	Jesi 1	1	3	63.2
	Moie	1	3	60.6
Oct-92	Jesi	1	2	42.0
Jan-94	Ancona	1	2	63.2
	Cupramontana 1	1	2	74.0
	Jesi 1	3	2	73.6
	Moie	3	2	47.0
Jul-94	Cupramontana 1	1	2	62.4
Sep-95	Moie	1	1	24.6
Mar-96	Moie	1	2	16.2
Apr-96	Jesi 1	2	4	55.2
Oct-96	Cupramontana 1	2	3	110.6
	Jesi 1	5	3	105.8
	Moie	3	3	76.6
Dec-96/Jan-97	Apiro	4	13	191.6
	Cupramontana 1	14	13	122.0
	Jesi 1	8	13	116.6
	Moie	7	13	142.6
Nov/Dec-98	Apiro	14	6	176.8
	Cupramontana 1	17	6	135.0
	Jesi 1	5	6	125.4
	Moie	12	6	128.8
	Poggio San Romualdo	2	6	76.4
Dec-99	Apiro	3	2	76.6
	Jesi 1	1	2	66.2
Jan-01	Jesi 1	1	5	80.8
	Cupramontana 1	1	5	68.8
Feb-04	Cupramontana 1	1	8	53.6
	Moie	1	8	44.2
Apr-05	Cupramontana 1	8	5	86.8
	Jesi 1	1	5	51.6
	Moie	3	5	37.8
May-05	Cupramontana 1	1	3	28.2
Oct-05	Ancona	1	4	49.6
	Cupramontana 1	2	4	58.0
	Jesi 1	3	4	67.8

Table 2 continued

Rainfall event (ID)	Station	Landslides	*D* (days)	*E* (mm)
Jan-06	Ancona	2	4	49.4
	Jesi 1	1	4	35.8
Apr-07	Ancona	1	2	31.6
Jun-07	Poggio San Giovanni	1	3	46.0
May-08	Jesi 2	2	5	70.2
Sep-08	Ancona	1	5	61.4
	Jesi	1	5	60.0
Dec-08	Agugliano	1	4	91.8
	Apiro	1	4	119.2
	Jesi 2	1	4	93.6
Jun-09	Agugliano	1	3	13.0
Jan-10	Agugliano	1	7	48.0
Feb-10	Moie	1	2	14.4
Mar-10	Jesi 2	1	3	33.8
	Moie	1	3	39.2
May-10	Agugliano	1	6	67.0
	Ancona	1	6	61.2
Dec-10	Agugliano	1	4	40.6
	Moie	1	4	55.2
Mar-11	Agugliano	4	11	149.0
	Ancona	1	11	164.4
	Fabriano	2	11	142.8
	Jesi 2	2	11	116.4
	Moie	6	11	144.0
	Poggio San Vicino	2	11	97.8
May-11	Ancona	1	3	39.6
		208		

For each rainfall event and rain gauge station, we report the number of triggered landslides, the rainfall duration (*D*), and the cumulative event rainfall (*E*)

Table 3 List of RCMs used in this study. All the RCMs share the same horizontal resolution of 12.5 km

Institute	RCM	Driving model	RCPs	References
KNMI	RACMO22E	EC-EARTH	4.5 8.5	Van Meijgaard et al. (2012)
SMHI	RCA4	CM5	4.5 8.5	Samuelsson et al. (2011)
CLMcom	CCLM4-8-17	CM5	4.5 8.5	Rockel et al. (2008)

potential future evolution of atmospheric composition. In fact, to different emission scenarios correspond different response of the climate system. In this regard, RCP 4.5 conceives a stabilization of the radiative forcing at 4.5 W m^{-2} thanks to mitigation policies undertaken to limit GHGs emission. A more "pessimistic" emission scenario is contemplated by the RCP 8.5, which considers the absence of climate change mitigation policies leading to a pathway of high GHGs emission and a subsequent higher radiative forcing of 8.5 W m^{-2}.

We chose 1971–2000 as historical period for calibrating the bias correction and for computing the climate change signal. This historical segment, different from the period of documented landslide occurrence (i.e., 1990–2012), has been chosen for the following reasons:

1. To properly calibrate the QDM correction function we sought for a 30-year time segment, needed for encompassing climate variability;
2. To filter out the effect of different radiative forcing assumed by the two RCPs we calibrate the QDM correction function over a period characterized by the same observed GHGs concentrations (in fact, the two RCP simulations are forced by observed GHGs concentration up to 2005);
3. To maximize the time span between historical and future period (2070–2099) and related changes, since we postulate a time-independent relationship between landslide occurrence and magnitude of triggering rainfall events.

3 Methods

3.1 Statistical post-processing of simulated rainfall

The simulated rainfall time series have been post-processed according to a QDM technique presented in Cannon et al. (2015). As explained below, QDM advances the traditional post-processing technique of quantile mapping (QM) (Boé et al. 2007; Dosio and Paruolo 2011; Berg et al. 2012; Gudmundsson et al. 2012; Casati et al. 2013; Wilcke et al. 2013; Smith et al. 2014) originally proposed by Panofsky and Brier (1968). Traditional QM aims at defining a quantile-specific transfer function computed by the mismatch between the observed and simulated cumulative distribution functions (CDFs) over a common historical series (i.e., calibration) generally with length $\geq$ 30 years. The transfer function is defined on a set of physical values corresponding to discrete quantiles, and then interpolated to correct all simulated physical values. QM is a valuable technique for bias correction and for downscaling climate simulations (Piani et al. 2010; Themeßl et al. 2011b; Berg et al. 2012; Gudmundsson et al. 2012), yet QM is also known to alter original simulated CCS (Themeßl et al. 2011a; Dosio et al. 2012; Maurer and Pierce 2014; Smith et al. 2014; Cannon et al. 2015; Switanek et al. 2017; Sangelantoni et al. 2018). The inflation or deflation of the original CCS could be physically plausible only in the case of a temporal stationarity of the model bias. Temporal stationarity means that the bias affecting present climate simulations is assumed unvarying in the future climate (Maraun 2013; Gaitan 2016; Switanek et al. 2017). Since establishing such a condition is beyond the scope of this work, we used QDM which represents one solution to circumvent artificial CCS alteration.

The first step of QDM consists of a quantile–quantile detrending of the time series that must be post-processed. It consists in deriving and then removing the quantile-specific relative change (i.e., trend). A quantile-specific relative change corresponds to the ratio between a simulated rainfall value at time t associated to a certain quantile (e.g., 95th) in the future period and the simulated rainfall value associated to the same quantile in the historical period. A simulated detrended value is then obtained by scaling the future rainfall value by its relative change.

In the second step, a traditional QM application is used to correct detrended simulation mapping of the statistical properties of the observed time series. Figure 5 shows the original and statistically adjusted simulations reproducing the statistical intensity of the observed rainfall over the historical temporal segment used as calibration period (1971–2000). Finally, the trend extracted in the first step is added back to the corrected time series derived from the second step, thus preserving the changes produced by the original simulation. Figure 6 shows a comparison between the CCS obtained with the original and the statistically adjusted simulations over different statistics. For this study, because landslide-triggering thresholds are derived from observed rainfall, it is important superimposing simulated trend to a simulation having the same statistical properties of the observed rainfall climatology. QDM accurately reproduced original CCS affecting the right tail of distribution of high to extreme rainfall events (potentially landslides). However, it was also observed an alteration of the original mean CCS. According to the QDM, this can be due to the multiplicative approach (i.e., correction factors are multiplied to the original simulation quantiles) in the case of a substantial difference of dry days frequency between historical and future time segments (Switanek et al. 2017).

We apply the QDM over two different temporal segments (see Sect. 4). First, the entire simulated period (1971–2099) for the analysis related to the ED model. Then, the QDM has been applied to the 1971–2000 and to the 2070–2099 temporal segments, for the analysis related to the Bayesian probabilistic model.

Finally, differently from Cannon et al. (2015), the QDM transfer functions have been defined on observations at station scale. In this configuration, the post-processing involves a simulation bias correction and downscaling to the station scale as well, considering the representativeness error arising from the spatial-scale mismatch between simulations and observations (Casati et al. 2013).

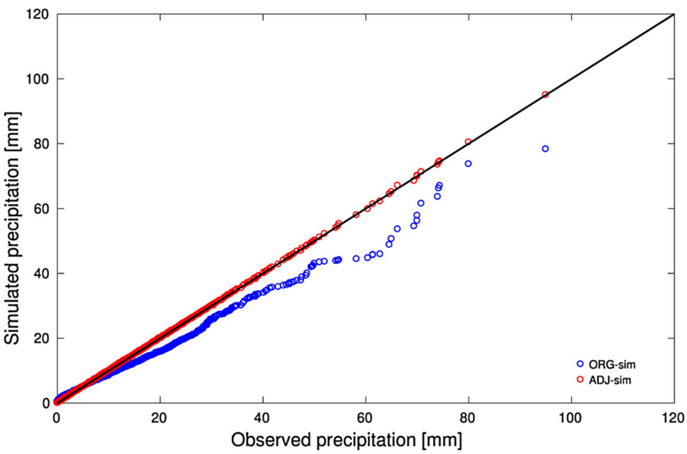

Fig. 5 Quantile–quantile mismatch between the original (blue) and statistically adjusted (red) simulated and observed rainfall over a common historical (i.e., calibration) period 1971–2000. This is exemplary shown for one RCM (RACMO22E) and one reference site (Ancona)

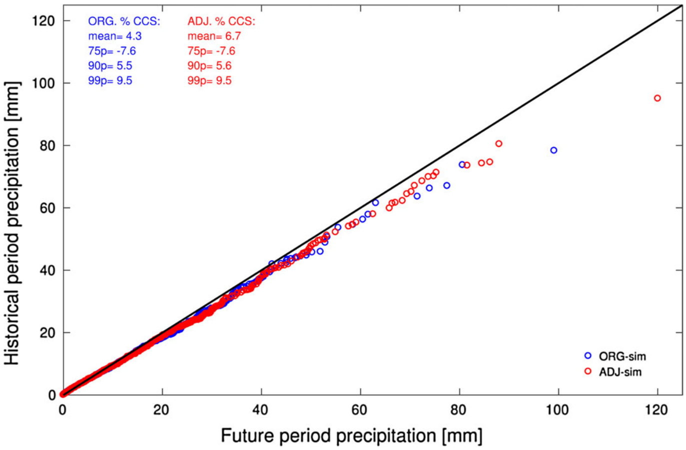

Fig. 6 Simulated rainfall quantile–quantile comparison between future period (2070–2099) and historical period (1971–2000), considering original (blue) and statistically adjusted (red) simulations. Text in the upper-left part of the plot reports CCS (percentage difference between the two periods) related to specific statistics obtained considering original and adjusted simulations. This is exemplary shown for one RCM (RACMO22E) and one reference site (Ancona)

3.2 Landslide predictive models

The literature in the subject of rainfall threshold for landslide occurrence is wide and characterized by different scale of analysis and rainfall-based proxies (Guzzetti et al. 2007, 2008; Segoni et al. 2018). A threshold is a mathematical relationship generally defined as "the minimum or maximum level of some quantity needed for a process to take place or a state to change" (White et al. 1996). For rainfall-induced landslides, a threshold may represent the limit (lower, midst, or upper) of the hydrological condition in which landslides are likely to occur (Reichenbach et al. 1998).

Among the most used techniques to determine the amount of rainfall needed to trigger landslides are the statistical rainfall threshold models, which assess the correlation between rainfall proxies and landslides through statistical analysis of historical records (Guzzetti et al. 2008). Indeed, the hydrogeological conditions in which our dataset of shallow landslides has occurred can be reasonably simplified by the statistical rainfall threshold models because their small dimensions allow to consider such landslides as a point, with relatively uniform characteristics, on a large scale (Cervi et al. 2010). In the statistical models, the threshold between rainfall and landslides that happened in the past is assumed to be also the threshold of future landslides (Martelloni et al. 2011).

In this study, for the definition of statistical rainfall thresholds across the selected study area, we consider four rainfall proxies [cumulative event rainfall (E), rainfall duration (D), daily rainfall (R), and 5-day antecedent rainfall (A_5)] applied to two different models: (1) the cumulative event rainfall–rainfall duration model (E–D proxies), and (2) the Bayesian probabilistic model (E–A_5 proxies).

3.2.1 The cumulative event rainfall–rainfall duration (ED) model

The cumulative event rainfall–rainfall duration (ED) model (Innes 1983; Sengupta et al. 2010; Vennari et al. 2014; Brunetti et al. 2015; Gariano et al. 2015) assumes that the threshold curve is a power law:

$$E = aD^b \tag{1}$$

where E is the cumulative event rainfall measured from the beginning to the end of the rainfall event in which one or more landslides were activated (mm), D is the duration of the rainfall event (day), and a and b are constants which control the shape of the curve.

Data of cumulative event rainfall and duration have been computed for the 68 rainfall events that triggered the 208 landslides considered (Fig. 7). Then, a technique suggested by Guzzetti et al. (2007) has been adopted to portray percentile estimates of the rainfall ED conditions. The purpose is to approximate the values at the empty data (i.e., bins) and to minimize the effect of clustering at specific duration. In fact, the ED chart reveals a bias in the database, especially for rainfall duration ranging from six to eleven days, possibly due to the unequal distribution of landslides throughout the analyzed period. Starting from the minimum value of D and up to the maximum, a sliding window of 11 bins has been isolated among the rainfall events. Therefore, at the nth duration value, a range of 11 data centered in the nth value (i.e., five bins to the left and five bins to the right of the central bin) has been considered. The 10th, 50th, and 95th percentiles of the cumulative rainfall for the selected events have been computed and attributed to the central point of the 11-bins moving window along the duration axis. Percentile lines are then drawn by joining equal percentile points (Fig. 7). Starting from these lines, the 10, 50, and 95% rainfall thresholds were computed in the form of power law regressions (Fig. 7). Such curves represent, respectively, the 10, 50, and 95% probability of landslide initiation (10p, 50p, and 95p, respectively) with determined ED conditions.

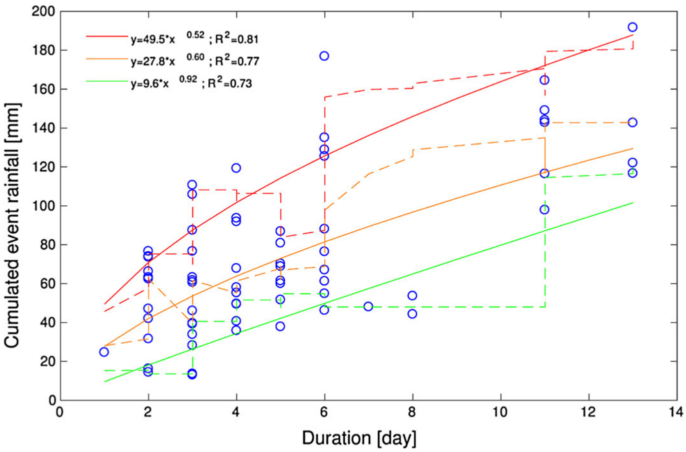

Fig. 7 Relation between cumulated rainfall and duration of the 68 rainfall events (blue circles) that triggered landslides in the study area. Dashed lines portray 10th (green), 50th (orange), and 95th (red) percentile estimates of rainfall ED conditions, while solid lines represent the 10% (green), 50% (orange), and 95% (red) probabilistic rainfall thresholds

In this study, the three landslides probability curves, produced by the observation-based statistical model, act as the reference thresholds to assess, over the period 1971–2099, the temporal evolution of the rainfall events with the 10, 50, and 95% probability of landslides initiation within the study area.

3.2.2 The Bayesian probabilistic model

The statistically based probabilistic models are mathematical models that use historical records of landslide occurrence to predict the probability of future landslides (Coe et al. 2004). These models incorporate variability and uncertainty, providing a quantitative assessment of threshold reliability (Bean 2009). One of the most applied approaches is the statistical Bayesian inference, firstly proposed by Guzzetti et al. (2005). In this work, the Bayesian probabilistic model is used adopting a two-dimensional application, as proposed in Berti et al. (2012):

$$P(L \vee R, A_5) = (P(R, A_5) \vee L) * P(L)/P(R, A_5) \quad (2)$$

where the probability $P(L|R, A_5)$ is the conditional probability of occurrence of at least one landslide (L) given a rainfall event of a fixed range of values of daily rainfall (R) and 5-day antecedent rainfall (A_5). $P(R, A_5|L)$ is the conditional probability of observing a rainfall event of magnitude (R, A_5) when a landslide occurs. $P(L)$ is the probability that at least one landslide occurs independently of the rainfall event. Finally, $P(R, A_5)$ is the probability of observing a rainfall event of magnitude (R, A_5) independently of the occurrence of a landslide.

This method is performed in terms of relative frequencies and returns a value of landslide probability (from 0 to 1) for each combination of the described parameters (R and A_5). To assess $P(L|R, A_5)$, we use 3 classes corresponding to 3 level of landslide probability that could be comparable to the ED thresholds: (1) 0–0.50 for low probability, (2) 0.51–0.95 for medium probability, and (3) $>$ 0.95 for high probability.

For this model we use the same landslides and rainfall datasets previously described. Given the importance of non-triggering rainfall events in a probabilistic study, we attempt to overcome the issue of probability underestimation by visualizing results only for the years in which at least one landslide has been reported. Furthermore, we interpolate rainfall data for the entire study area instead of using the punctual information deriving from the rain gauges. Despite the well-known resulting problems of data flattering, such decision allows us to consider the totality of landslides in a single analysis thus increasing statistical reliability. Table 4 shows the results of the interpolation for the landslides-triggering rainfall events, which are recognizable by the same ID used in Table 2.

Values of $P(L|R, A_5)$ have been plotted in a (R, A_5) plane delimited by intervals of 0–19.9 mm, 20.0–39.9 mm, 40.0–59.9 mm, and $\geq$ 60.0 mm (Fig. 8). For example, the lower-left box of the figure represents the probability of initiating at least one landslide, given a rainfall event of $0 \leq R \leq 19.9$ mm and $0 \leq A_5 \leq 19.9$ mm. The colors of the histograms correspond to levels of landslide probability: low (green), medium (orange), and high (red). The "not applicable" boxes (NA, gray) indicate rainfall conditions that never occurred in the study area during the considered period.

In this study, the above-described landslide probability classes (LPCs), assigned to each combination of (R, A_5), have been used to compare the variation in landslide occurrence over the periods 1971–2000 and 2070–2099.

Table 4 Results of the interpolation for the rainfall events that triggered at least one landslide within the study area

Rainfall event (ID)	Landslides	Date (yyyy/mm/dd)	R (mm)	A_5 (mm)
Dec-90	5	1990/12/14	9.7	74.9
	25	1990/12/15	2.4	74.3
Sep-91	1	1991/09/28	0.0	14.1
Nov-91	4	1991/11/24	68.4	29.5
Oct-92	1	1992/10/20	33.6	26.3
Jan-94	8	1994/01/20	50.7	16.5
Jul-94	1	1994/07/20	36.6	0.4
Sep-95	1	1995/09/08	18.0	17.5
Mar-96	1	1996/03/16	18.4	11.9
Apr-96	2	1996/04/03	18.0	23.7
Oct-96	4	1996/10/08	48.2	21.2
	4	1996/10/09	22.2	68.0
	2	1996/10/10	0.2	90.0
Dec-96/Jan-97	5	1996/12/30	3.2	77.3
	13	1996/12/31	1.9	62.5
	4	1997/01/01	12.7	50.8
	2	1997/01/02	3.0	51.3
	7	1997/01/03	3.9	43.6
	2	1997/01/04	3.9	24.7
Nov/Dec-98	43	1998/12/01	62.7	26.4
	6	1998/12/02	3.2	89.0
	1	1998/12/04	32.2	89.3
Dec-99	4	1999/12/15	51.8	10.3
Jan-01	2	2001/01/30	41.5	27.8
Feb-04	2	2004/02/27	8.8	28.4
Apr-05	1	2005/04/10	30.6	5.6
	7	2005/04/12	2.3	67.2
	4	2005/04/13	0.0	69.5
May-05	1	2005/05/18	7.2	12.4
Oct-05	5	2005/10/08	55.4	22.1
	1	2005/10/09	4.7	69.3
Jan-06	3	2006/01/03	29.3	18.2
Apr-07	1	2007/04/05	0.8	31.8
Jun-07	1	2007/06/08	0.4	29.3
May-08	2	2008/05/20	45.7	6.0
Sep-08	1	2008/09/13	11.1	5.5
	1	2008/09/14	11.8	16.6
Dec-08	1	2008/12/12	56.9	29.1
	2	2008/12/13	0.6	86.0
Jun-09	1	2009/06/01	37.2	52.2
Jan-10	1	2010/01/03	2.5	28.2
Feb-10	1	2010/02/06	4.5	9.2

Table 4 continued

Rainfall event (ID)	Landslides	Date (yyyy/mm/dd)	R (mm)	A_5 (mm)
Mar-10	1	2010/03/10	19.0	20.7
	1	2010/03/11	2.7	36.6
May-10	2	2010/05/16	6.9	75.4
Dec-10	2	2010/12/01	24.0	79.7
Mar-11	4	2011/03/01	53.1	13.3
	2	2011/03/02	42.7	66.4
	2	2011/03/03	9.5	109.1
	1	2011/03/06	0.8	114.5
	3	2011/03/08	0	19.5
	5	2011/03/09	0	10.0
May-11	1	2011/05/17	0	30.1
	208			

For each rainfall event, we report the number of triggered landslides, the daily rainfall (R), and the 5-days antecedent rainfall (A_5)

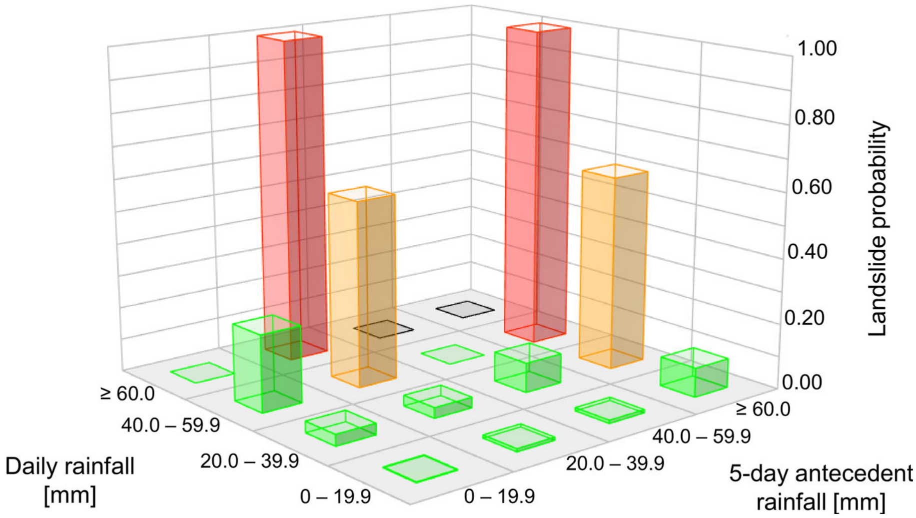

Fig. 8 Histograms of landslide probability for different combinations of (R, A_5). Colors represent the corresponding LPC: low (green), medium (orange), high (red), and NA (gray)

4 Analyses

The landslide initiation models and the rainfall simulations explained above were combined to perform two different analyses to highlight future annual and seasonal changes in landslides occurrence (autumn: October, November, December; winter: January, February, March; spring: April, May, June; summer: July, August, September).

The first analysis considers the temporal evolution (1971–2099) of the events above rainfall thresholds (EARTh) for landslide initiation, which represent rainfall events (rainfall event $\geq$ 1 mm and duration $\geq$ 1 day) above the three thresholds derived from the

ED statistical model. The annual (or seasonal) number of EARTh has been normalized to the total number of annual (or seasonal) rainfall events. In this way, we derive the relative frequency of potential landslide initiation events. Trends are evaluated applying a linear regression model to the annual (or seasonal) EARTh time series. The statistical significance of these trends is verified with the Mann–Kendall test (Wilks 2006). A further complementary analysis addresses the change in rainfall probability distribution functions (PDFs) between the historical (1971–2000) and the future (2070–2099) temporal segments. Differently from the previous, this complementary analysis considers also smaller rainfall events not exceeding the landslide initiation thresholds. Rainfall events have been clustered in equal-sized bins, representing rainfall of a certain cumulative and duration class. Rainfall events placed above the 10p, 50p, and 95p thresholds signify the PDF of the EARTh. These results are accessible in the enclosed supplementary materials (Figs. SM 2–4).

The second analysis compares the variation in landslide occurrence between the historical (1971–2000) and future (2070–2099) temporal segments. The number of expected rainfall events belonging to each LPC derived from the Bayesian model has been computed for both temporal segments. Finally, seven landslide variation classes (LVCs), from − 3 to + 3, have been defined to evaluate the increment or decrease in expected landslide movements (Table 5).

4.1 Trends of the events above rainfall thresholds (EARTh)

The EARTh trends over the three reference sites chosen for the Esino basin are shown in Figs. 9, 10 and 11. Each subplot includes results from three RCMs forced by the RCP 4.5 (dashed lines) and RCP 8.5 (solid lines), highlighting possible effects of different GHGs concentration over landslide-triggering rainfall. Here, we discuss the annual and the seasonal trends during winter and summer. The trends for autumn and spring are available in the supplementary materials (Fig. SM 1).

The trend of every EARTh and their statistical significance are summarized in the matrix of Table 6. To rate the p values, we use the following symbols: p values ≥ 0.05 not statistically significant (blank/no asterisk); p values < 0.05 statistically significant (*); p values < 0.01 moderately statistically significant (**); p values < 0.001 highly statistically significant (***).

Results show a general increase in the EARTh frequencies over time. Similarly, all the significant trends show increasing slopes. The RCP 8.5 scenarios produced a larger number of increasing and significant trends in both the annual and seasonal analyses. However, the sensitivity to the different GHG emission scenarios varies according to the RCM

Table 5 Class of variation related to the different landslide probability class

LVC	Variation (%)
3	> 100
2	[51:100]
1	[1:50]
0	0
− 1	[− 50:1]
− 2	[− 100:− 51]
− 3	< − 100

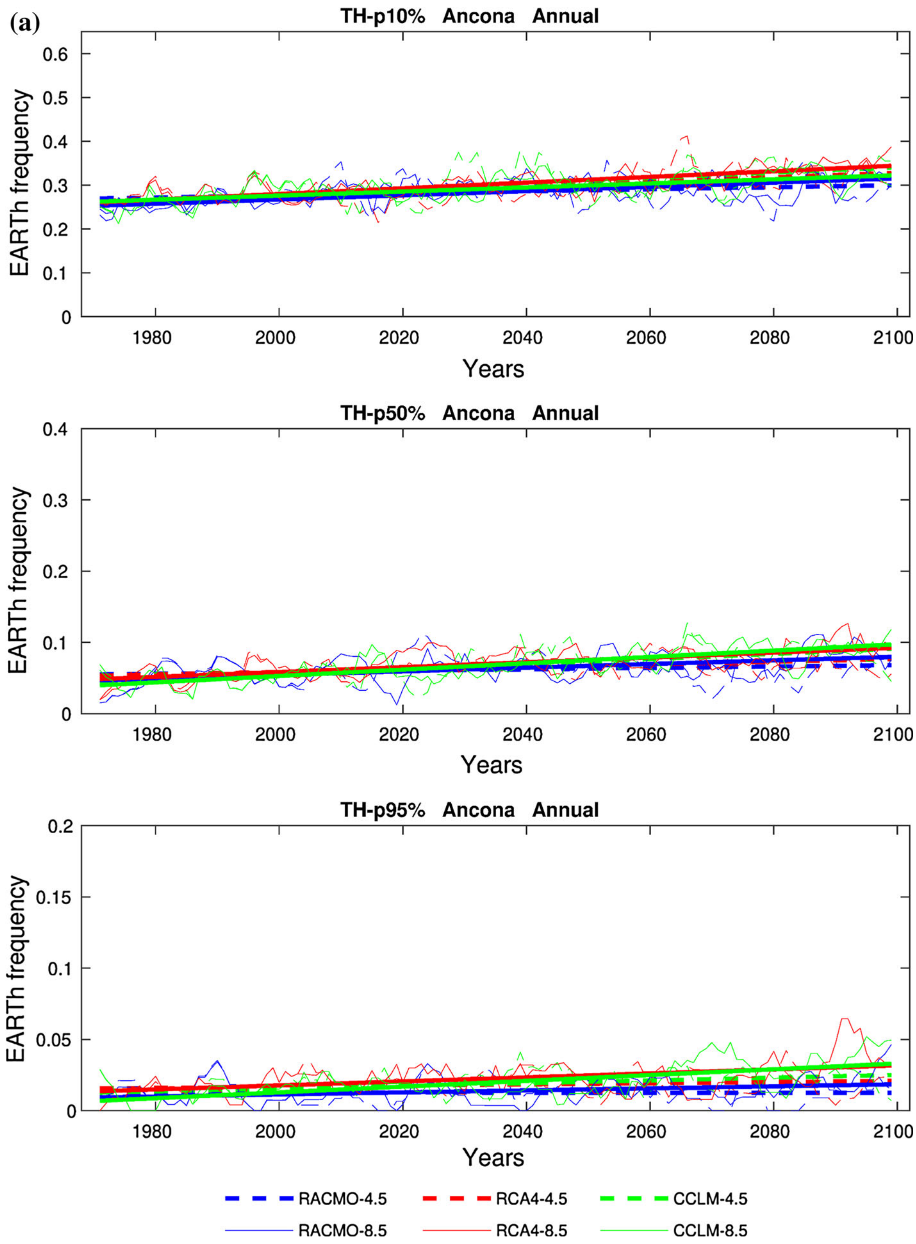

Fig. 9 Temporal evolution (5-year running mean), with the linear regression, of annual events above rainfall thresholds (EARTh) relative frequency. EARTh are computed in respect to the three thresholds for each of the three reference sites of the Esino basin (**a** for Ancona, **b** for Jesi, and **c** for Apiro). Each subplot includes results of three RCMs run with two different radiative forcing represented by the RCP 4.5 (dashed lines) and RCP 8.5 (solid lines)

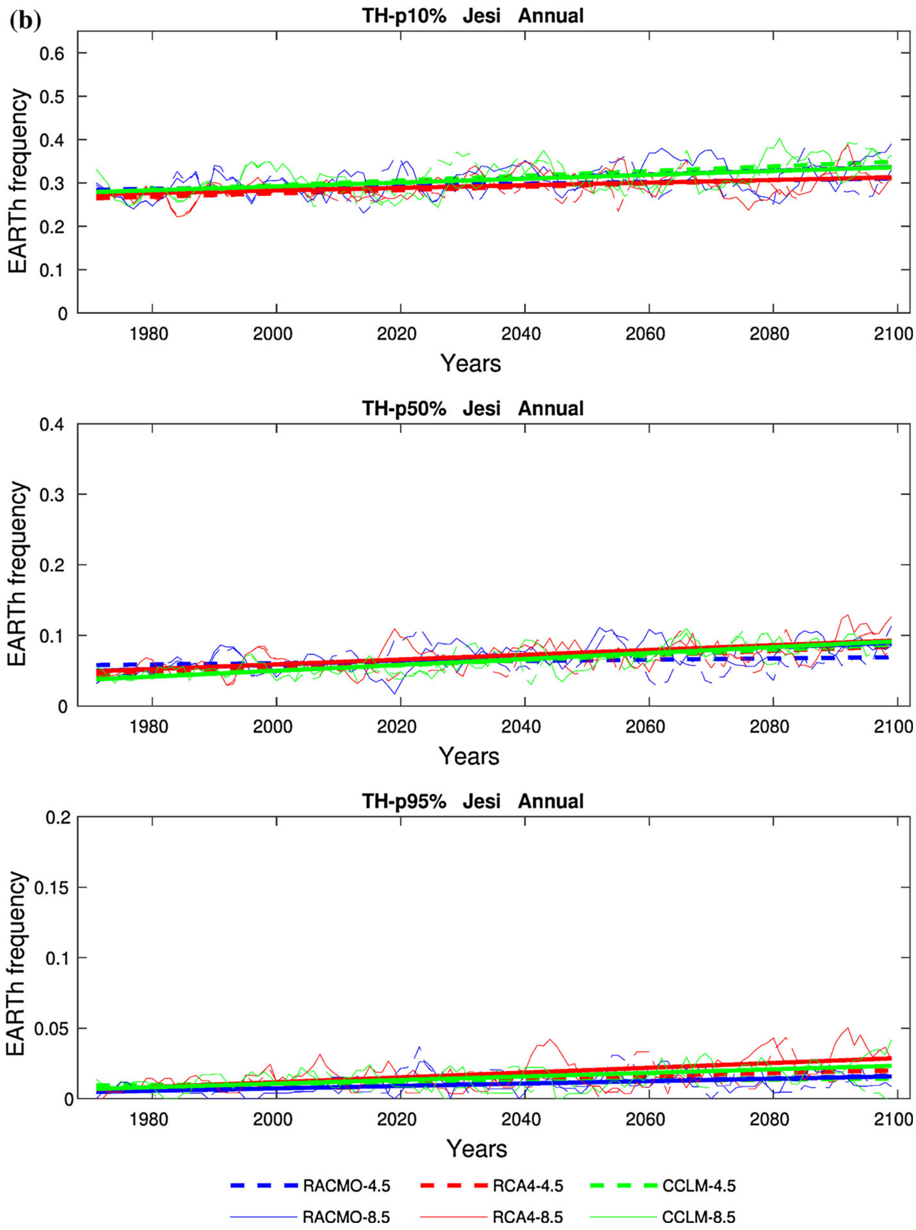

Fig. 9 continued

considered. For instance, considering annual analysis, RACMO displays the larger sensitivity to the different RCP considered, because many negative trends in the RCP 4.5 became positive in the RCP 8.5 (Table 6). On the other hand, RCA4 and CCLM reveal a more comparable RCP-sensitivity because driven by the same global climate model (GCM; i.e., CNRM-CM5).

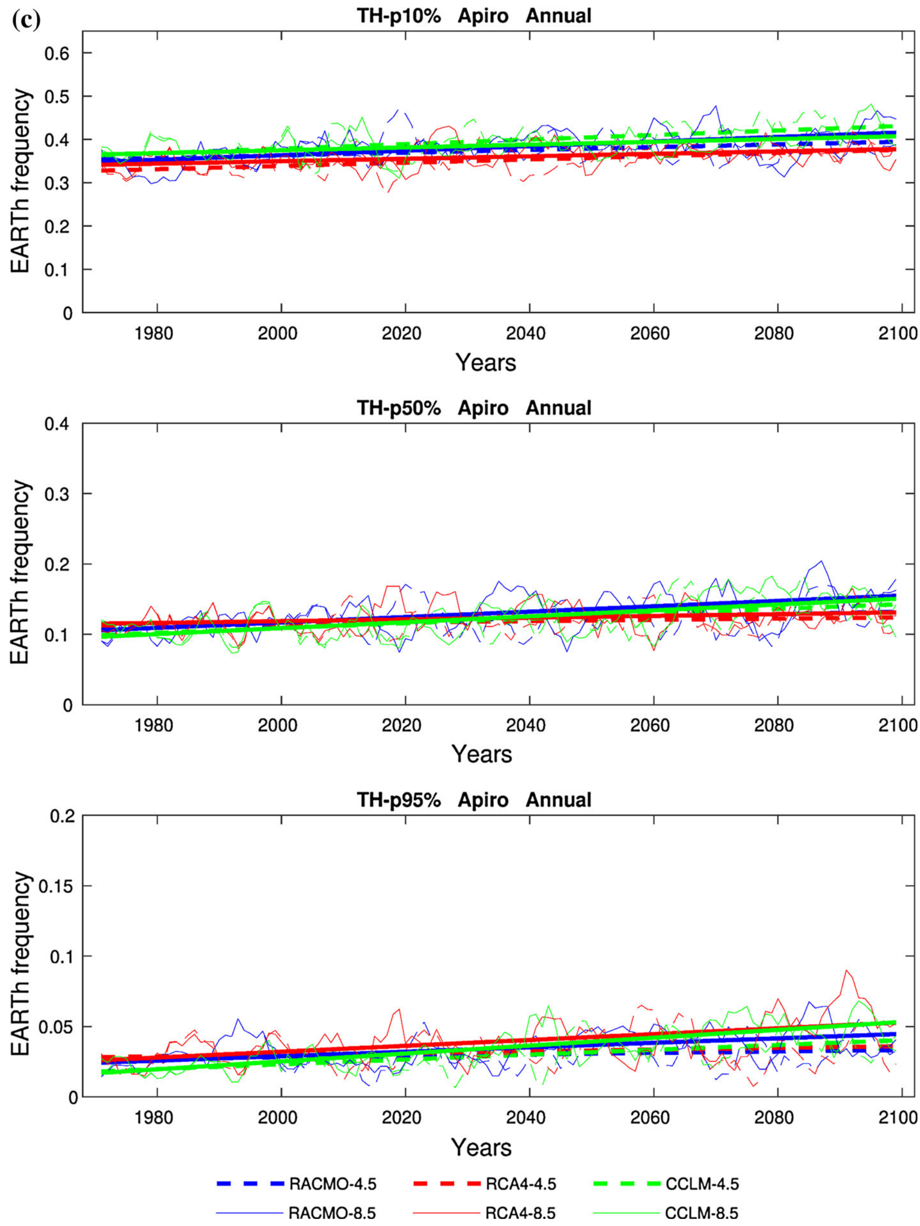

Fig. 9 continued

The analysis of the annual 10p-EARTh (i.e., rainfall events that exceed the 10% probability to initiate a landslide) highlights relative frequencies lower than 0.3 for the coast site (Fig. 9a) and lower than 0.4 for the mountain site (Fig. 9c). Increasing trends with similar magnitude are visible both in the RCMs and on the studied sites. Moreover, such trends appear of comparable magnitude toward the end of twenty-first century tallying

Table 6 Table shows, for each temporal base (Annual (Ann)–Winter (Win)–Summer (Sum)), reference station, RCM, and RCP, the trend of every ELTEs and their statistical significance

	Ancona			Jesi			Apiro		
	Ann	Win	Sum	Ann	Win	Sum	Ann	Win	Sum
RACMO 4.5									
10p									
50p									
95p									
RCA 4.5									
10p	**		*	*	*		**	***	
50p	*			**				**	
95p				*					
CCLM 4.5									
10p	**			**			**	**	
50p	***		**	***		*	**		
95p	*						**		
RACMO 8.5									
10p	**			**			**	*	
50p	**			***			***		
95p				*			**		
RCA 8.5									
10p	***		*	*					
50p	***		*	***		*			
95p	*		*	***		*	**		
CCLM 8.5									
10p	**			**			*		
50p	***			***		**	***		*
95p	***		*	*			***		*

The colors indicate upward (light blue), null (gray), or backward (orange) trends. The asterisk rating system indicates p values ≥ 0.05 not statistically significant (blank), p values < 0.05 statistically significant (*), p values < 0.01 statistically moderately significant (**), p values < 0.001 statistically highly significant (***)

frequency of $\sim$ 0.3 in the coastal and $\sim$ 0.4 in mountain sites. However, the results of the Mann–Kendall test (Table 6) for the RCP 8.5 scenario simulations show larger number of significant trends compared to those of the RCP 4.5 scenario. The analysis of the annual 50p-EARTh (moving to more intense rainfall events) displays larger differences between

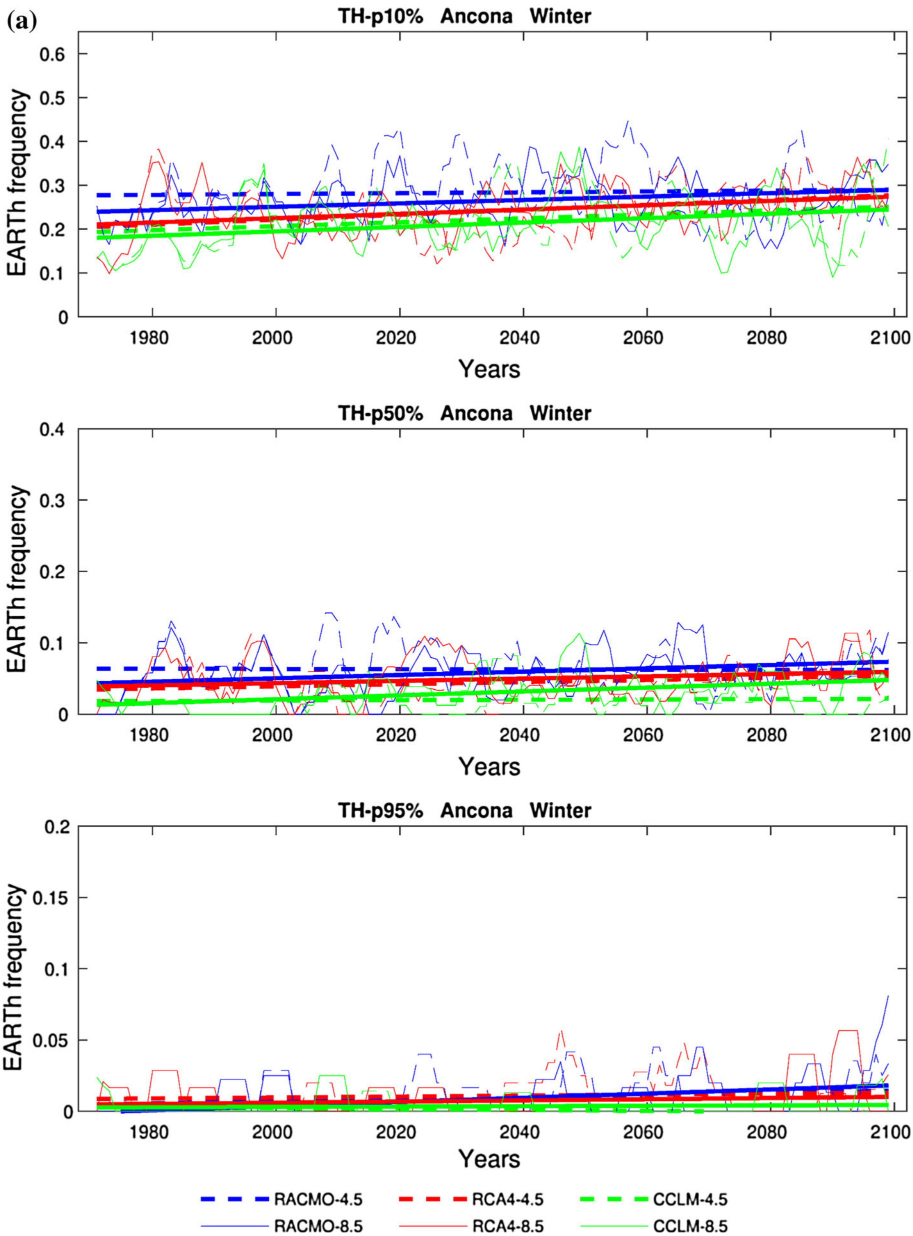

Fig. 10 Same as Fig. 9a–c but for winter season

the RCMs and studied sites. Higher EARTh frequency can be observed in the mountain site, approximately doubling the coast and hill sites frequency (Fig. 9a, b, respectively). However, too larger frequency in the mountain site do not correspond to increasing trend in that same site. Comparable to the 10p-EARTh also the 50p rainfall threshold shows steeper significant trends with the RCP 8.5-forced simulations when compared to the RCP 4.5

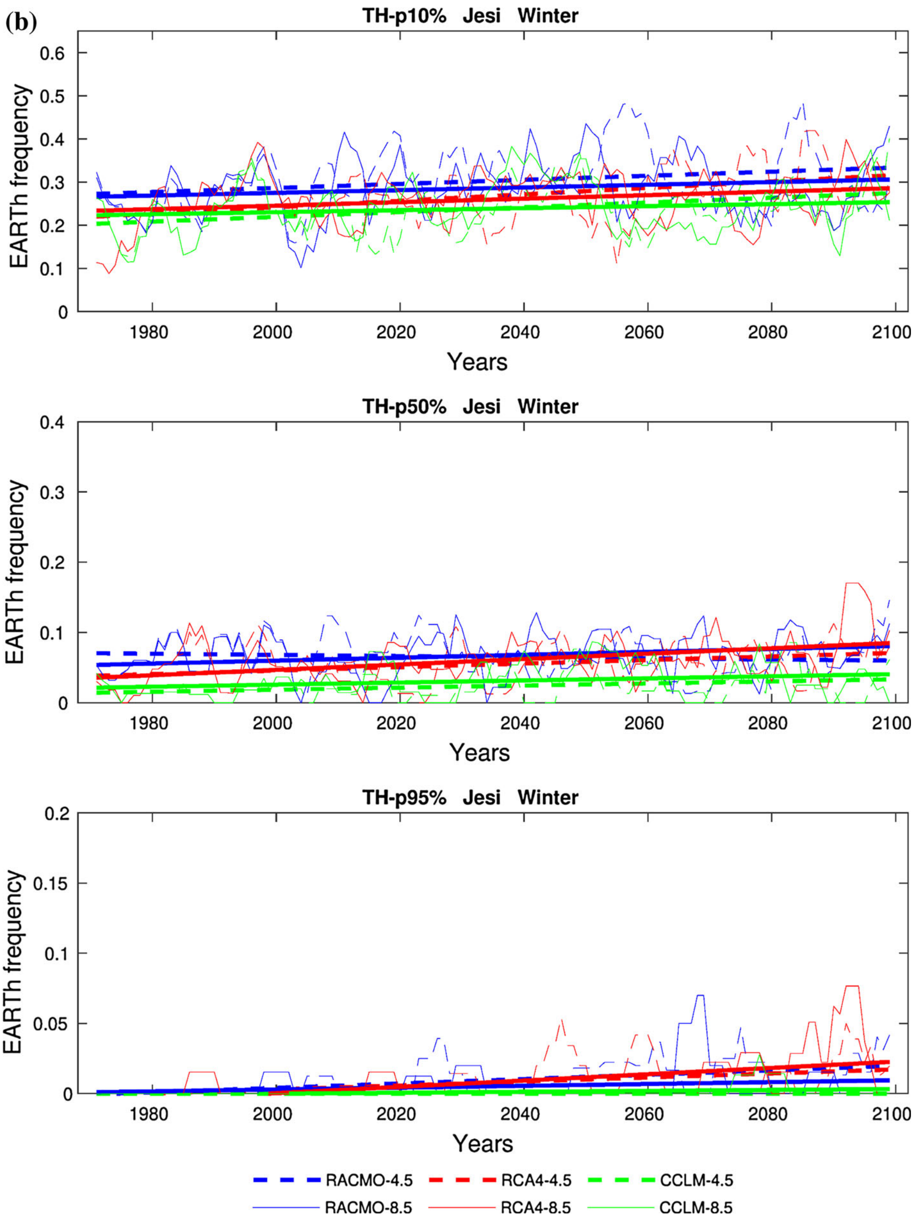

Fig. 10 continued

scenario. The relative frequency increases from $\sim$ 0.1 to $\sim$ 0.15 in the mountain reference site. The analysis of the annual 95p-EARTh (ranging from severe-to-extreme rainfall) reveals abundant statistically significant trends (Table 6). The signal is joined by large discrepancies between the two RCPs. This result indicates larger sensitivity in the 95p-EARTh to a different GHGs concentration. Another important aspect to stress is the

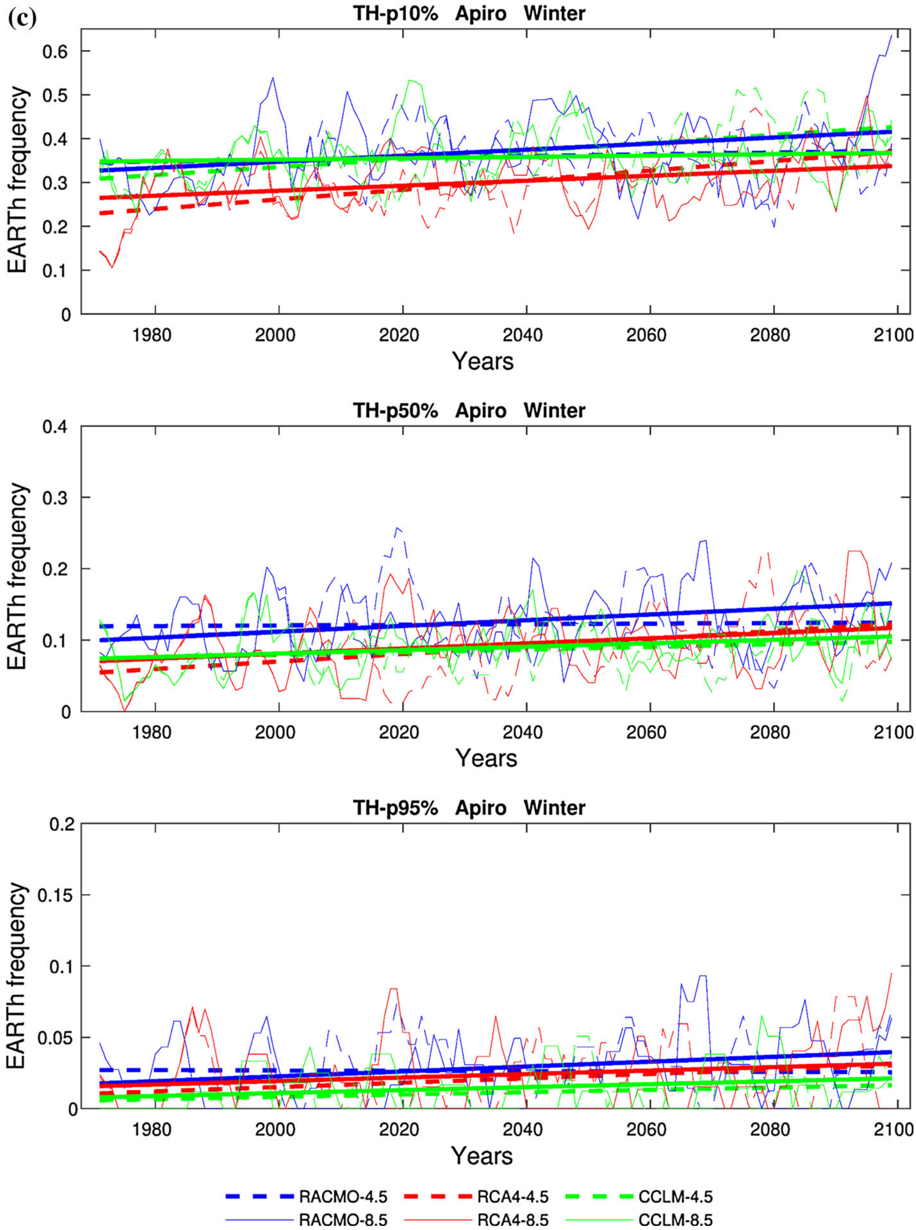

Fig. 10 continued

increase in inter-model spread (commonly considered as uncertainty metric in climate projections) with severe-to-extreme events. Over the three studied climate sectors, the mountain site shows the larger EARTh frequency, which in the RCP 8.5 scenario increased from a relative frequency of ~ 0.025 to ~ 0.05, over the entire temporal segment analyzed.

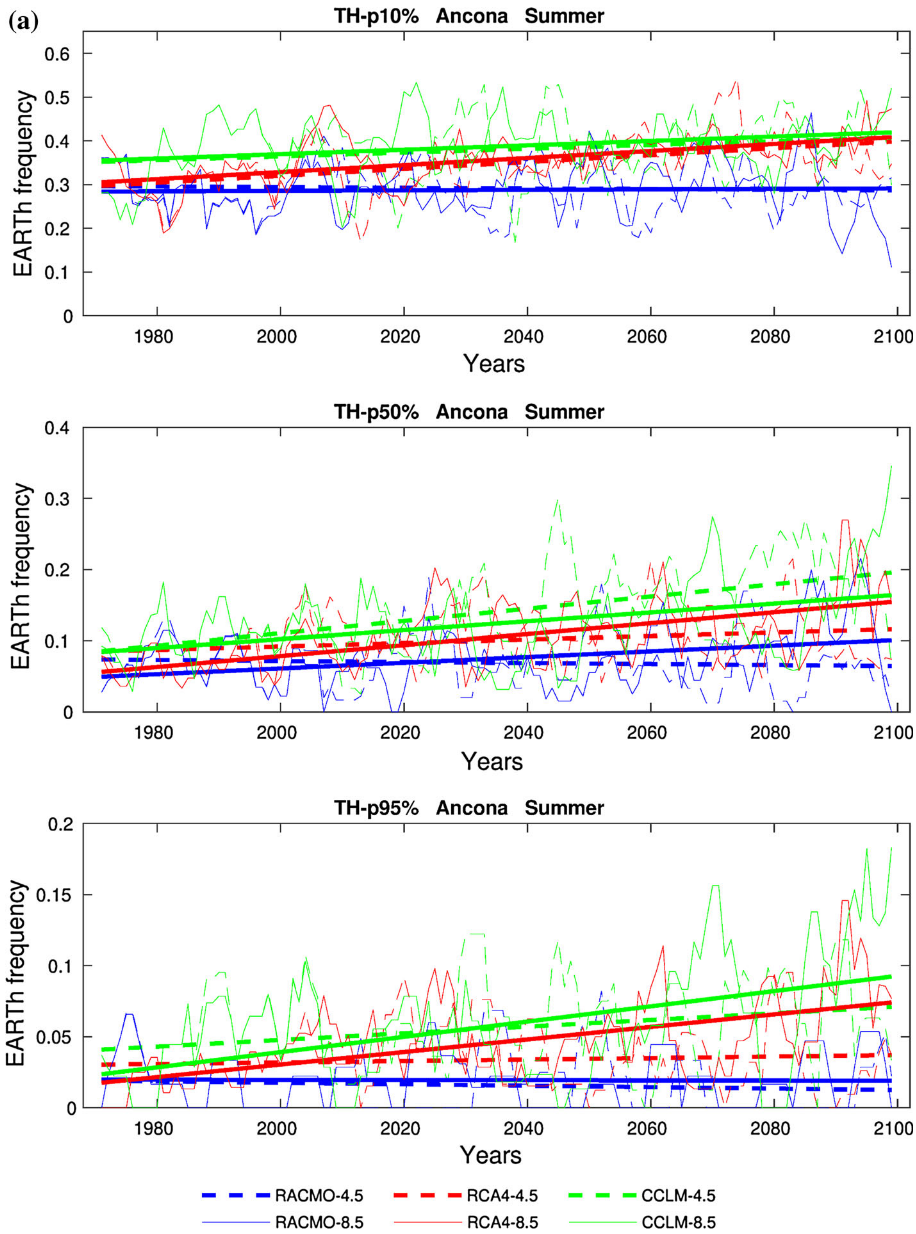

Fig. 11 Same as Fig. 9a–c but for summer season

Regardless of the considered rainfall threshold (10p, 50p, or 95p), the evolution of the EARTh appears strongly influenced by seasonal patterns. In winter, we obtained the smallest absolute number of EARTh especially with the 95p threshold, both in the coast and hill sites (Fig. 10a, b, respectively). Concerning the temporal evolution, most of the resulting trends are not significant, except for some instances in the 10p- and 50p-EARTh

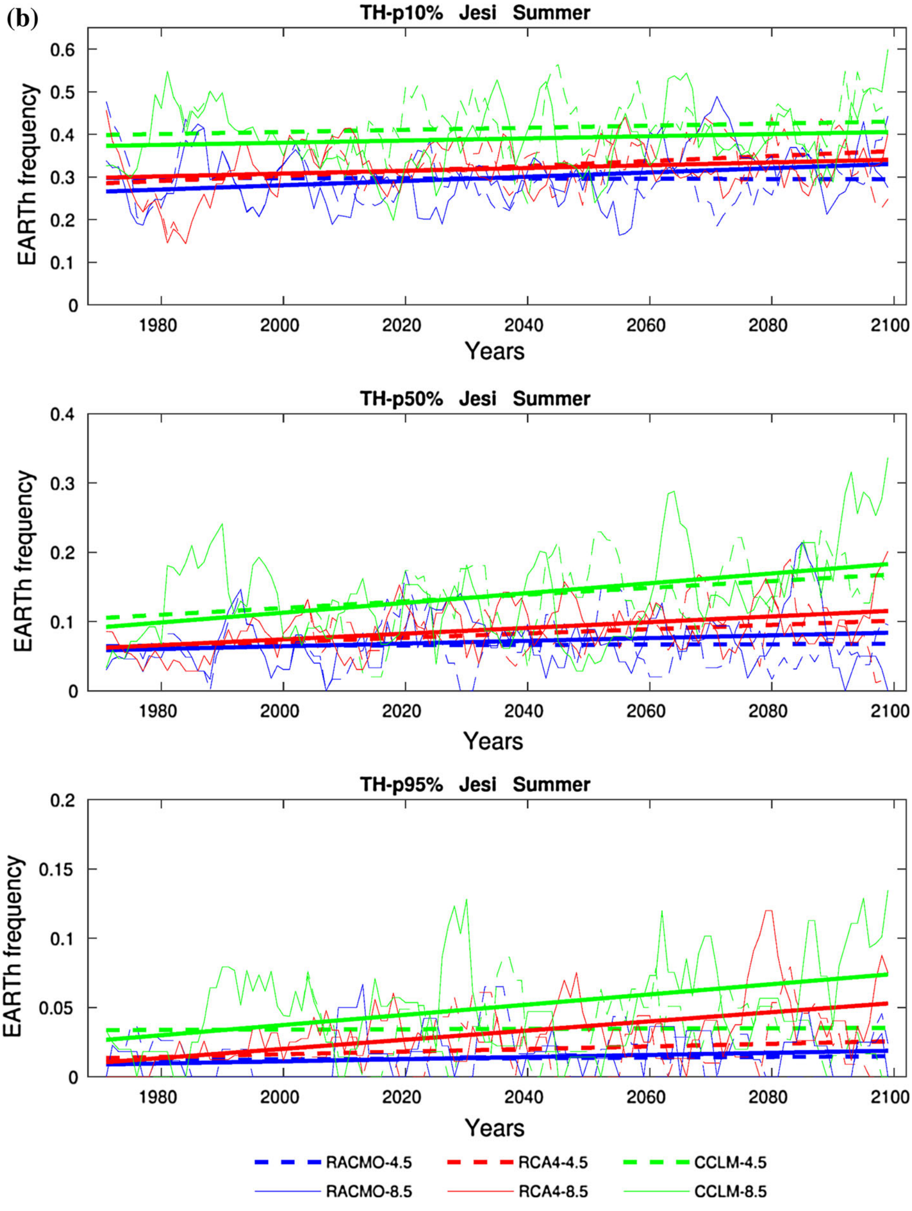

Fig. 11 continued

obtained in the RCP 4.5 scenario in the mountain site of Apiro (Fig. 10c and Table 6). The same site also projects larger 95p EARTh frequency toward the end of the twenty-first century ($\sim$ 0.025). In addition, we notice homogeneous increasing trends in the three RCMs and no evident alterations of the trends' magnitude connected to the expected changes in GHGs concentration considered in scenarios RCP 4.5 and RCP 8.5.

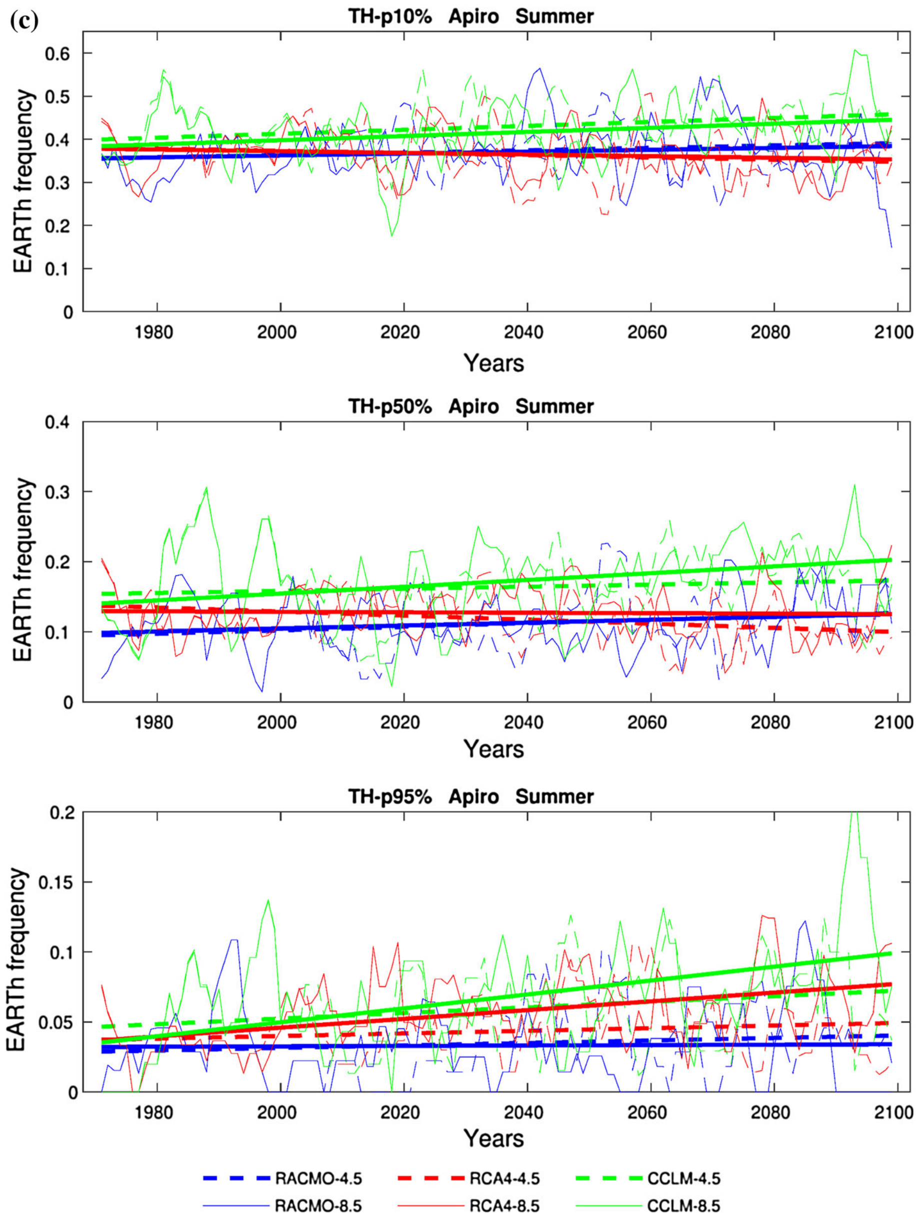

Fig. 11 continued

Winter rainfall in our area of study is mainly driven by Mediterranean cyclones and rarely triggered landslides. Changes may be expected in the future, since climate model projections indicate that Mediterranean cyclones will decrease in frequency but increase in intensity (Zappa et al. 2014; Scoccimarro et al. 2016). Nevertheless, according to the

RCMs considered, these expected changes in rainfall do not entail significant alterations of landslide-triggering events frequency.

Summer rainfall (Fig. 11), on the contrary, shows the largest relative frequency of EARTh regardless of the threshold considered. Noticeably, this season is also the most uncertain in terms of change signal discrepancies among the different thresholds, RCMs, RCPs, and studied sites. Furthermore, can be observed how summer EARTh trends are characterized by a large inter-annual variability, particularly over the 95p threshold.

In this context, the RCA4 and CCLM RCP 8.5 scenarios show a substantial increase in the 95p EARTh, mainly over the coastal and mountainous sites (Fig. 11a, c, respectively) compared to the hill one (Fig. 11b). In these sites, a relative frequency of $\sim$ 0.1 ($\sim$ 10% of events will exceed the 95p threshold) by the end of the twenty-first century is expected according to the CCLM RCM. However, consistent 95p EARTh increase is visible only in the two RCMs forced by the same driving GCM. In fact, much flatter trends result in the three thresholds for the RACMO RCM.

It is noteworthy that the RCA and CCLM positive trends obtained with the RCP 8.5 scenario are in contrast whit the much flatter trends resulting from the RCP 4.5. This suggests that, subjected to a larger warming, the atmosphere can hold amounts of moisture sustaining more intense landslide-triggering rainfall events (Pall et al. 2007; Giorgi et al. 2011; Drobinski et al. 2016; Volosciuk et al. 2016). At the same time, results of summer season shed light on how the representation of summer intense rainfall events, generally originated by convective processes, strongly depends on the RCM and RCP considered.

4.2 Future variation of landslide probability (Bayes)

The variation in landslide occurrence, between the historical (1971–2000) and the future (2070–2099) temporal segments considered in this study, is derived from the Bayesian model. Figure 12 shows results of the analyses on annual and seasonal (winter-summer) basis and for all the considered stations (Ancona, Jesi, and Apiro).

The graphs display for every LPC (horizontal axis) the corresponding LVC (vertical axis), both for RCP 4.5 (blue) and RCP 8.5 (red) scenarios. The number of expected rainfall events belonging to each (R, A_5) combination and the percentage of variation between the historical and the future periods are highlighted. The plot of each LPC shows the cumulative minimum, maximum, and median values of the corresponding LVCs according to all the three RCMs. Figure 12 represents the aggregate projection of increase or decrease in landslide initiation for each probability class.

Overall, results of the comparison between historical and future periods show a general increase in the landslide-triggering rainfall events. In fact, as it can be noticed the median of the cumulative number of rainfall events is expected to increase especially for the medium and high LPCs and the RCP 8.5. This translates into an intensification of the rainfall that are most likely to trigger landslides in the study area. Such outcomes are comparable with the general results of the EARTh analysis and with those of other similar studies (Jakob and Lambert 2009; Melchiorre and Frattini 2012; Turkington et al. 2016). Interestingly, this consideration is valid also for the NA class, thus indicating the possible occurrence of extreme rainfall with a magnitude never occurred during the historical period of the Bayesian model. Furthermore, the figure shows the most scattered values (highest spread between the minimum and maximum values) in the coastal site both on annual and seasonal basis and regardless of the LPC, witnessing the most uncertain change signal. This result is different from what obtained in the EARTh trends analysis, which did not present substantial differences across the studied sites.

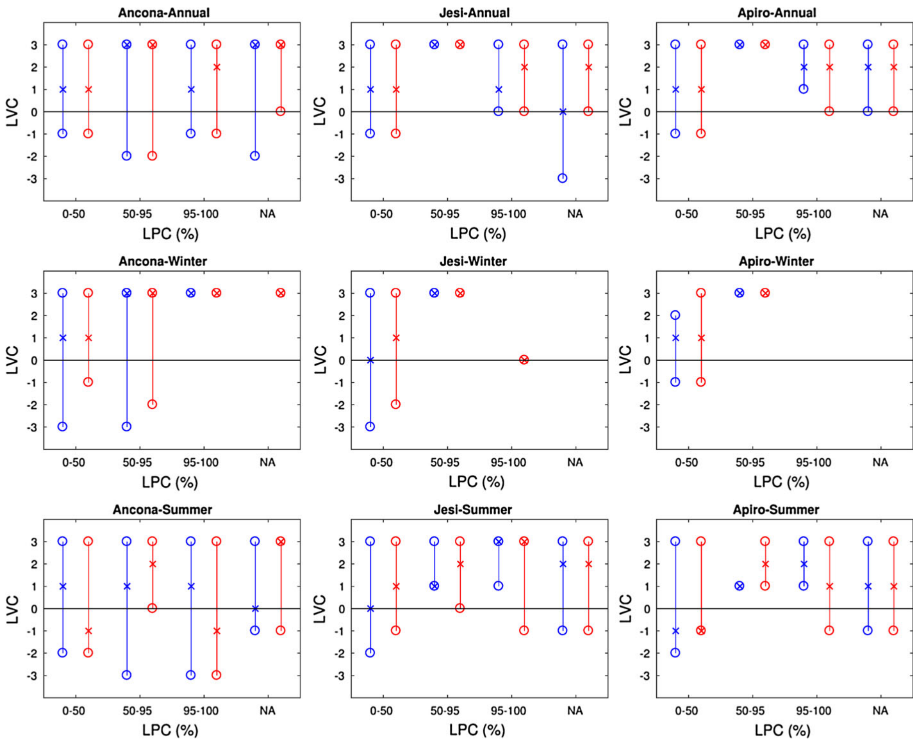

Fig. 12 Cumulative data scattering (minimum, maximum, and median values) of the LVCs (vertical axis) relative to each LPC (horizontal axis), measured as the percentage difference of the number of expected rainfall events in the future (2070–2099) and in the historical (1971–2000) periods. The subplots display the annual and seasonal analyses of all the stations and for both RCP 4.5 (blue) and RCP 8.5 (red)

Considering the annual analysis, it is readily noticeable that almost all the median and maximum values of LVCs are positive, while the minima are equally distributed between negative and zero values. This indicates an overall increment of the rainfall events among all the considered LPCs. Moreover, the dispersion in the low probability class is identical for all the stations and RCPs. Differently, in the medium and high probability classes, the mountain station shows the least data scattering and the highest median change values. Specifically, the medians of the second LPC are in class 3 (LVC $> 100\%$) for all stations, except for Ancona, which presents negative minima. In the third LPC, the coast-hill-mountain increasing discrepancies are even more emphasized. Such outcomes suggest an exacerbation of the rainfall events over the future thirty-year period, particularly the extreme ones which are more likely to trigger one or more landslides, especially in the mountain area. This result is consistent with the EARTh trends analysis.

The Bayesian probabilistic model points out also a significant seasonal pattern analogous to that found with trends analysis. Results for the winter season show the lowest spread. This is evident for the second, the third, and the NA probability classes, particularly in the hill and mountain stations. In most of these cases, the LVCs values coincide with class 3, thus indicating that all RCMs agree on the $> 100\%$ increase in the rainfall events with medium–high-extreme probability of landslide initiation. This is in line with the work of Ciabatta et al. (2016) in Umbria and Gariano et al. (2017) in Calabria (Southern Italy). It is also noteworthy to clarify that the blank spots represent the cases in which the variation could not be calculated; no rainfall event showed such (R, A_5) characteristics over the historical or future period. Indeed, the winter rainfall regime is characterized by frontal systems connected to large-scale circulations, generally producing rainfall spread over prolonged times. These systems should be subjected to minor changes in the future, as previously mentioned in Sect. 4.1.

Differently from the winter season, summer shows the highest variability over the LVCs, the LPCs, and across the three stations. The elevated dispersion of data is related to the uncertainty of the climate models' outcomes for such season. Interestingly, and differently from the other results, summer presents also major differences between RCP 4.5 and RCP 8.5. In fact, most of the minimum and median values of LVCs changes with the emission scenario; in general, the RCP 8.5 shows higher values than the RCP 4.5 except for the coastal site of Ancona. This confirms the results of the EARTh trend analysis and the uncertainty associated to the RCM results in the coastal area (Déqué et al. 2007; Zollo et al. 2014; Ciabatta et al. 2016).

5 Conclusions

In this study, statistically adjusted simulated rainfall was used to assess future landslide trends in the Esino river basin, Central Italy, through the end of the twenty-first century. We investigated possible changes in landslide-triggering rainfall patterns by means of three RCM simulations driven by two different emission scenarios (RCP 4.5 and RCP 8.5), in coastal, hilly and mountainous sites (Ancona, Jesi, and Apiro, respectively). Then, we performed landslide occurrence analysis using two statistical models run on four rainfall proxies. The first model couples cumulative event rainfall and rainfall duration proxies (EARTh analysis) to determine the projected temporal evolution of rainfall events exceeding three chosen landslide-triggering thresholds (10p, 50p, and 95p). The considered time interval was 1971–2099. The second model calculated the percentage variation in landslide probability between the historical (1971–2000) and a future (2070–2099) time periods. The model used four thresholds (low, medium, high, and NA) providing specific intervals of the daily rainfall and 5-day antecedent rainfall proxies (Bayesian analysis).

Both analyses projected an overall increase in landslides occurrence in the Esino river basin throughout the twenty-first century. This result was particularly marked for the RCP 8.5 scenario. The EARTh analysis showed that all the significant trends are positive, even if the sensitivity to the different RCPs varied significantly according to the RCMs considered. Moreover, the Bayesian analysis displayed positive median and maximum values of LVCs, thus indicating an overall increment of the rainfall events among all the LPCs.

On an annual basis, both statistical models revealed discrepancies among RCPs and RCMs in correspondence of the higher thresholds, thus shedding uncertainty over future landslides trends. However, all analyses indicated a larger increasing number of landslides in the mountain site in respect to the hill and coast sites. Finally, while the Bayesian investigation showed higher data scattering in the coastal site, the EARTh analysis did not present substantial differences in the inter-model spread across the studied sites.

Results also showed considerable differences between the summer and the winter seasons, in terms of RCMs agreement and change signal magnitude. In winter, both analyses recognized rather uniform increasing landslide-triggering rainfall trends without evident sensitivity to the RCP considered. However, results showed moderately dissimilar change signal magnitude between the landslide models. In fact, we obtained flatter and not statistically significant EARTh trends, but over 100% increase in the rainfall events with medium–high probability of landslide initiation in the Bayesian analysis. Furthermore, the latter revealed the possible occurrence of extreme rainfall with a magnitude never occurred during the historical period. Differently from the winter season, the summer change signals exhibit very large variability through the different landslide thresholds, RCMs, RCPs, and study sites. Indeed, the discrepancies of the RCMs found in the EARTh analysis are visible also in the Bayesian model. Similarly, in both statistical models' analysis, the RCP 8.5 scenario shows larger change signal compared to those of RCP 4.5. On the other hand, concerning the spatial patterns, the major increase in summer landslides occurrence is expected in the coast and mountain sectors (Ancona and Apiro, respectively) with the ED-model, while is expected in the hill sector (Jesi) with the Bayesian model.

Besides the projected increase in landslide occurrence in the study area, the results of this study testify the complexity of defining a comprehensive characterization of possible changes. Three main sources of uncertainty can be identified: (1) the selection and the number of the climate simulations considered, which should be possibly maximized to get more comprehensive representation of the potential evolution of the atmosphere; (2) the statistical post-processing technique used to reduce climate simulation biases, which should be carefully evaluated in function of the climate information required for the specific impact considered; (3) the impact model(s), here generally intended as the (statistical or deterministic) model which is fed or combined to the climatic forcing. On this last issue, by using two different landslide initiation models we emphasized the concordant (i.e., robust) and discordant (i.e., uncertainty) aspects of the changes affecting landslides frequency provided by the two analyses. Consequently, the choice of the statistical model which translates climate simulations into the expected impacts should be carefully evaluated and chosen in function of the climate service required by the end users.

In the end, we are aware that landslides initiation depends not only on climate, but also on many other variables belonging to both the natural and the anthropic spheres. Nonetheless, we believe that feeding climate projections into landslide predictive models represents a proficient tool for decision makers also applicable on different spatial and temporal scales. In fact, the methodology here applied to long-term climate projections could be also used with short-term projections and seasonal forecasts over geologically uniform regions.

Acknowledgements Authors are grateful to the EURO-CORDEX modeling community that produced the climate simulations used in this paper (http://www.euro-cordex.net/) and to the Earth System Grid Federation for hosting these data (https://esg-dn1.nsc.liu.se/projects/esgf-liu/). We also want to thank Cannon et al. (2015) for making freely available the simulations bias correction technique (https://cran.r-project.org/web/packages/MBC/MBC.pdf). Furthermore, we acknowledge the support of the Marche Region's Civil Protection Monitoring and Forecasting Center (Department for Integrated Security and Civil Protection Policies of the Marche Region) for providing the observational rainfall and landslides datasets. Finally, we would like to thank the anonymous reviewers for the constructive comments that greatly improved the manuscript.

Appendix

Variables and acronyms used in the text

Variable	Description	Unit
A_5	5-day antecedent rainfall	mm
D	Rainfall duration	day
E	Cumulative event rainfall	mm
L	Landslide event (one or more)	–
R	Daily rainfall	mm

Acronym	Description
CCS	Climate change signal
EARTh	Events above rainfall thresholds
GCM	Global circulation model
GHG	Greenhouse gas
LPC	Landslide probability class
LVC	Landslide variation class
PDF	Probability density function
QDM	Quantile delta mapping
QM	Quantile mapping
RCM	Regional climate model
RCP	Representative concentration pathway

References

Aleotti P (2004) A warning system for rainfall-induced shallow failures. Eng Geol 73:247–265. https://doi.org/10.1016/j.enggeo.2004.01.007

Appiotti F, Krželj M, Russo A, Ferretti M, Bastianini M, Marincioni M (2014) A multidisciplinary study on the effects of climate change in the northern Adriatic Sea and the Marche region (Central Italy). Reg Environ Change 14:2007–2024. https://doi.org/10.1007/s10113-013-0451-5

Bean MA (2009) Probability: the science of uncertainty with applications to investments, insurance, and engineering. American Mathematical Society, Pacific Grove

Bellprat O, Kotlarski S, Lüthi D, Schär C (2013) Physical constraints for temperature biases in climate models. Geophys Res Lett 40:4042–4047. https://doi.org/10.1002/grl.50737

Berg P, Feldmann H, Panitz HJ (2012) Bias correction of high resolution regional climate model data. J Hydrol 448–449:80–92. https://doi.org/10.1016/j.jhydrol.2012.04.026

Berti M, Martina MLV, Franceschini S, Pignone S, Simoni A, Pizziolo M (2012) Probabilistic rainfall thresholds for landslide occurrence using a Bayesian approach. J Geophys Res 117:20. https://doi.org/10.1029/2012JF002367

Bindoff NL, Stott PA, AchutaRao KM, Allen MR, Gillett N, Gutzler D, Hansingo K, Hegerl G, Hu Y, Jain S, Mokhov II, Overland J, Perlwitz J, Sebbari R, Zhang X (2013) Detection and attribution of climate change: from global to regional. In: Climate Change 2013: The Physical Science Basis. Contribution of Working Group I to the Fifth Assessment Report of the Intergovernmental Panel on Climate Change. Cambridge University Press, Cambridge, United Kingdom and New York, NY, USA

Bisci C, Dramis F (1991) La geomorfologia delle Marche. In: Minetti A, Nanni T, Perilli F, Polonara L, Principi M (ed) L'ambiente Fisico delle Marche. SELCA, Firenze, pp 83–103

Boberg F, Christensen JH (2012) Overestimation of Mediterranean summer temperature projections due to model deficiencies. Nat Clim Change 2:433–436. https://doi.org/10.1038/nclimate1454

Boé J, Terray L, Habets F, Martin E (2007) Statistical and dynamical downscaling of the Seine basin climate for hydro-meteorological studies. Int J Climatol 1655:1643–1655. https://doi.org/10.1002/joc

Brunetti MT, Peruccacci S, Antropico L, Bartolini D, Deganutti AM, Gariano SL, Iovine G, Lucani S, Luino F, Melillo M, Palladino MR, Parise M, Rossi M, Turioni L, Vennari C, Vessia G, Viero A, Guzzetti F (2015) Catalogue of rainfall events with shallow landslides and new rainfall thresholds in Italy. In: Lollino G, Giordan D, Crosta GB, Corominas J, Azzam R, Wasowski J, Sciarra N (eds) Engineering geology for society and territory. Volume 2—landslide processes. Springer, Berlin, pp 1575–1579

Cannon AJ, Sobie SR, Murdock TQ (2015) Bias correction of GCM precipitation by quantile mapping: how well do methods preserve changes in quantiles and extremes? J Clim 28:6938–6959. https://doi.org/10.1175/JCLI-D-14-00754.1

Cardinali M, Guzzetti F (eds) (2003) Carta Inventario dei Movimenti Franosi della Regione Marche ed aree limitrofe. Pubblicazione CNR GNDCI, Perugia

Casati B, Yagouti A, Chaumont D (2013) Regional climate projections of extreme heat events in nine pilot Canadian communities for public health planning. J Appl Meteorol Climatol 52:2669–2698. https://doi.org/10.1175/JAMC-D-12-0341.1

Cervi F, Berti M, Borgatti L, Ronchetti F, Manenti F, Corsini A (2010) Comparing predictive capability of statistical and deterministic methods for landslide susceptibility mapping: a case study in the northern Apennines (Reggio Emilia Province, Italy). Landslides 7:433–444. https://doi.org/10.1007/s10346-010-0207-y

Christensen JH, Boberg F, Christensen OB, Lucas-Picher P (2008) On the need for bias correction of regional climate change projections of temperature and precipitation. Geophys Res Lett 35:L20709. https://doi.org/10.1029/2008GL035694

Ciabatta L, Camici S, Brocca L, Ponziani F, Stelluti F, Berni N, Moramarco T (2016) Assessing the impact of climate-change scenarios on landslide occurrence in Umbria Region, Italy. J Hydrol 541:285–295. https://doi.org/10.1016/j.jhydrol.2016.02.007

Coe JA, Godt JW (2012) Review of approaches for assessing the impact of climate change on landslide hazards. In: Eberhardt E, Froese C, Turner AK, Leroueil S (eds) Landslides and engineered slopes, protecting society through improved understanding, proceedings 11th international and 2nd North American symposium on landslides and engineered slopes, Banff, Canada. Taylor & Francis Group, London, pp 371–377

Coe J, Michael J, Crovelli RA, Laprade WT, Nashem WD (2004) Probabilistic assessment of precipitation-triggered landslides using historical records of landslide occurrence, Seattle, Washington. Environ Eng Geosci X:103–122

Crozier MJ (1996) The climate-landslide couple: a Southern Hemisphere perspective. Paleoclimate Res 19:329–350

Crozier MJ (2010) Deciphering the effect of climate change on landslide activity: a review. Geomorphology 124:260–267. https://doi.org/10.1016/j.geomorph.2010.04.009

De Vita P, Reichenbach P (1998) Rainfall-triggered landslides: a reference list. Environ Geol 35:219–233. https://doi.org/10.1007/s002540050308

Déqué M, Rowell DP, Lüthi D, Giorgi F, Christensen JH, Rockel B, Jacob D, Kjellström E, de Castro M, van den Hurk M (2007) An intercomparison of regional climate simulations for Europe: assessing uncertainties in model projections. Clim Chang 81:53–70. https://doi.org/10.1007/s10584-006-9228-x

Dikau R, Schrott L (1999) The temporal stability and activity of landslides in Europe with respect to climatic change (TESLEC): main objectives and results. Geomorphology 30:1–12. https://doi.org/10.1016/s0169-555x(99)00040-9

Dosio A, Paruolo P (2011) Bias correction of the ENSEMBLES high-resolution climate change projections for use by impact models: evaluation on the present climate. J Geophys Res 116:D16106. https://doi.org/10.1029/2011JD015934

Dosio A, Paruolo P, Rojas R (2012) Bias correction of the ENSEMBLES high resolution climate change projections for use by impact models: analysis of the climate change signal. J Geophys Res Atmos 117:1–24. https://doi.org/10.1029/2012JD017968

Drobinski P, Da Silva N, Panthou G, Bastin S, Muller C, Ahrens B, Borga M, Conte D, Fosser G, Giorgi F, Güttler I (2016) Scaling precipitation extremes with temperature in the Mediterranean: past climate assessment and projection in anthropogenic scenarios. Clim Dyn. https://doi.org/10.1007/s00382-016-3083-x

European Commission (2004) Global Land Cover for the Year 2000. In: Bartholomé E, Belward A, Beuchle R, Eva H, Fritz S, Hartley A, Mayaux P, Stibig H-J (eds) Luxembourg Office for Official Publications of the European Communities, catalogue number LB-55-03-099-ENC

Folchi Vici D'Arcevia C, Nanni T, Palpacelli S, Siciliani A, Vita F, Vivalda P (2008) Schema Idrogeologico della Regione Marche, Foglio Nord, Scala 1:100.000. Regione Marche—Servizio Ambiente e Paesaggio, Ancona

Gaitan CF (2016) Effects of variance adjustment techniques and time- invariant transfer functions on heat wave duration indices and other metrics derived from downscaled. Nat Hazards 83:1661–1681. https://doi.org/10.1007/s11069-016-2381-2

Gariano SL, Guzzetti F (2016) Landslides in a changing climate. Earth Sci Rev 162:227–252. https://doi.org/10.1016/j.earscirev.2016.08.011

Gariano SL, Brunetti MT, Iovine G, Melillo M, Peruccacci S, Terranova O, Vennari C, Guzzetti F (2015) Calibration and validation of rainfall thresholds for shallow landslide forecasting in Sicily, Southern Italy. Geomorphology 228:653–665. https://doi.org/10.1016/j.geomorph.2014.10.019

Gariano SL, Rianna G, Petrucci O, Guzzetti F (2017) Assessing future changes in the occurrence of rainfall-induced landslides at a regional scale. Sci Total Environ 596–597:417–426. https://doi.org/10.1016/j.scitotenv.2017.03.103

Gennaretti F, Sangelantoni L, Grenier P (2015) Toward daily climate scenarios for Canadian Arctic coastal zones with more realistic temperature-precipitation interdependence. J Geophys Res Atmos 120:11,862–11877. https://doi.org/10.1002/2015jd023890

Gentili B, Dramis F (eds) (1997) Geomorphology and Quaternary Evolution of Central Italy—Guide for the excursion. Suppl Geogr Fis Dinam Quat 3:79–103

Gioia E, Carone T, Marincioni F (2015) Rainfall and land use empirically coupled to forecast landslides in the Esino river basin, central Italy. Nat Hazards Earth Syst Sci 15:1289–1295. https://doi.org/10.5194/nhess-15-1289-2015

Giorgi F (1990) Simulation of regional climate using a limited area model nested in a general circulation model. J Clim 3:941–963

Giorgi F, Coppola E (2010) Does the model regional bias affect the projected regional climate change? An analysis of global model projections. Clim Change 100:787–795. https://doi.org/10.1007/s10584-010-9864-z

Giorgi F, Mearns LO (1999) Introduction to special section: regional climate modeling revisited. J Geophys Res 104:6335. https://doi.org/10.1029/98JD02072

Giorgi F, Jones C, Asrar GR (2009) Addressing climate information needs at the regional level: the CORDEX framework. WMO Bull 58:175–183

Giorgi F, Im ES, Coppola E, Diffembaugh NS, Gao XJ, Mariotti L, Shy Y (2011) Higher hydroclimatic intensity with global warming. J Clim 24:5309–5324. https://doi.org/10.1175/2011JCLI3979.1

Gudmundsson L, Bremnes JB, Haugen JE, Engen-Skaugen T (2012) Technical note: downscaling RCM precipitation to the station scale using statistical transformations—a comparison of methods. Hydrol Earth Syst Sci 16:3383–3390. https://doi.org/10.5194/hess-16-3383-2012

Guzzetti F, Peruccacci S, Rossi M (2005) Definition of critical threshold for different scenarios (WP 1.16). IRPI-CNR, Perugia

Guzzetti F, Peruccacci S, Rossi M, Stark C (2007) Rainfall thresholds for the initiation of landslides in central and southern Europe. Meteorol Atmos Phys 98:239–267. https://doi.org/10.1007/s00703-007-0262-7

Guzzetti F, Peruccacci S, Rossi M, Stark CP (2008) The rainfall intensity–duration control of shallow landslides and debris flows: an update. Landslides 5:3–17. https://doi.org/10.1007/s10346-007-0112-1

Hawkins E, Sutton R (2009) The potential to narrow uncertainty in regional climate predictions. Bull Am Meteorol Soc 90:1095–1107. https://doi.org/10.1175/2009BAMS2607.1

Innes JL (1983) Debris flows. Prog Phys Geogr 7:469–501

Jacob D, Petersen J, Eggert B, Alias A, Christensen OB, Bouwer LM, Braun A, Colette A, Déqué M, Georgievski G, Georgopoulou E, Gobiet A, Menut L, Nikulin G, Haensler A, Hempelmann N, Jones C, Keuler K, Kovats S, Kröner N, Kotlarski S, Kriegsmann A, Martin E, van Meijgaard E, Moseley C, Pfeifer S, Preuschmann S, Radermacher C, Radtke K, Rechid D, Rounsevell M, Samuelsson P, Somot S, Soussana JF, Teichmann C, Valentini R, Vautard R, Weber B, Yiou P (2014) EURO-CORDEX: new high-resolution climate change projections for European impact research. Reg Environ Change 14:563–578. https://doi.org/10.1007/s10113-013-0499-2

Jakob M, Lambert S (2009) Climate change effects on landslides along the southwest coast of British Columbia. Geomorphology 107:275–284. https://doi.org/10.1016/j.geomorph.2008.12.009

Lenton TM, Held H, Kriegler E, Hall JW, Lucht W, Rahmstorf S, Schellnhuberet HJ (2008) Tipping elements in the Earth's climate system. Proc Natl Acad Sci USA 105:1786–1793. https://doi.org/10.1073/pnas.0705414105

Lorenz DJ, DeWeaver ET (2007) The response of the extratropical hydrological cycle to global warming. J Clim 20:3470–3484. https://doi.org/10.1175/JCLI4192.1

Maraun D (2013) Bias correction, quantile mapping, and downscaling: revisiting the inflation issue. J Clim 26:2137–2143. https://doi.org/10.1175/JCLI-D-12-00821.1

Mariotti A, Struglia MV, Zeng N, Lau KM (2002) The hydrological cycle in the mediterranean region and implications for the water budget of the Mediterranean Sea. J Clim 15:1674–1690. https://doi.org/10.1175/1520-0442(2002)015<1674:THCITM>2.0.CO;2

Martelloni G, Segoni S, Fanti R, Catani F (2011) Rainfall thresholds for the forecasting of landslide occurrence at regional scale. Landslides 9:485–495. https://doi.org/10.1007/s10346-011-0308-2

Martinotti ME, Pisano L, Marchesini I, Rossi M, Peruccacci S, Brunetti MT, Melillo M, Amoruso G, Loiacono P, Vennari C, Vessia G, Trabace M, Parise M, Guzzetti F (2017) Landslides, floods and sinkholes in a karst environment: the 1–6 September 2014 Gargano event, Southern Italy. Nat Hazards Earth Syst Sci 17:467–480. https://doi.org/10.5194/nhess-17-467-2017

Maurer EP, Pierce DW (2014) Bias correction can modify climate model simulated precipitation changes without adverse effect on the ensemble mean. Hydrol Earth Syst Sci 18:915–925. https://doi.org/10.5194/hess-18-915-2014

McInnes R, Jakeways J, Fairbank H, Mathie E (eds) (2007) Landslides and climate change: challenges and solutions. In: Proceedings of the international conference on landslides and climate change. Taylor & Francis, Ventnor. https://doi.org/10.1201/noe0415443180

Meinshausen M, Smith SJ, Calvin K, Daniel JS, Kainuma MLT, Lamarque JF, Matsumoto K, Montzka SA, Raper SCB, Riahi K, Thomson A, Velders GJM, van Vuuren DPP (2011) The RCP greenhouse gas concentrations and their extensions from 1765 to 2300. Clim Change 109:213–241. https://doi.org/10.1007/s10584-011-0156-z

Melchiorre C, Frattini P (2012) Modelling probability of rainfall-induced shallow landslides in a changing climate, Otta, Central Norway. Clim Change 113:413–436. https://doi.org/10.1007/s10584-011-0325-0

Moss RH, Edmonds JA, Hibbard KA, Manning MR, Rose SK, van Vuuren DP, Carter TR, Emori S, Kainuma M, Kram T, Meehl GA, Mitchell JFB, Nakicenovic N, Riahi K, Smith SJ, Stouffer RJ, Thomson AM, Weyant JP, Wilbanks TJ (2010) The next generation of scenarios for climate change research and assessment. Nature 463:747–756. https://doi.org/10.1038/nature08823

National Institute of Statistics—ISTAT (2016) Population by age, sex and marital status on 1 January 2017. http://demo.istat.it/pop2016/index.html. Accessed 14 Sept 2017

Pall JS, Allen MR, Stone DA (2007) Testing the Clausius–Clapeyron constraint on changes in extreme precipitation under CO_2 warming. Clim Dyn 28:351–363. https://doi.org/10.1007/s00382-006-0180-2

Panofsky HA, Brier GW (1968) Some applications of statistics to meteorology. The Pennsylvania State University, University Park

Peruccacci S, Brunetti MT, Luciani S, Vennari C (2012) Lithological and seasonal control on rainfall thresholds for the possible initiation of landslides in central Italy. Geomorphology 139–140:79–90. https://doi.org/10.1016/j.geomorph.2011.10.005

Piani C, Weedon GP, Best M, Gomes SM, Viterbo P, Hagemann S, Haerter JO (2010) Statistical bias correction of global simulated daily precipitation and temperature for the application of hydrological models. J Hydrol 395:199–215. https://doi.org/10.1016/j.jhydrol.2010.10.024

Pisano L, Zumpano V, Malek Z, Rosskopf CM, Parise M (2017) Variations in the susceptibility to landslides, as a consequence of land cover changes: a look to the past, and another towards the future. Sci Total Environ 601–602:1147–1159

Reichenbach P, Cardinali M, De Vita P, Guzzetti F (1998) Regional hydrological thresholds for landslides and floods in the Tiber River Basin (central Italy). Environ Geol 35:146–159. https://doi.org/10.1007/s002540050301

Riahi K, Rao S, Krey V, Cho C, Chirkov V, Fischer G, Kindermann G, Nakicenovic N, Rafaj P (2011) RCP 8.5—a scenario of comparatively high greenhouse gas emissions. Clim Change 109:33–57. https://doi.org/10.1007/s10584-011-0149-y

Rockel B, Will A, Hense A (2008) Special issue regional climate modelling with COSMO-CLM (CCLM). Meteorol Z 17:347–348. https://doi.org/10.1127/0941-2948/2008/0309

Samuelsson P, Jones C, Willén U, Ullerstig A, Gollvik S, Hansson U, Jansson C, Kjellstrom E, Nikulin G, Wyser K (2011) The rossby centre regional climate model RCA3: model description and performance. Tellus A 63:4–23. https://doi.org/10.1111/j.1600-0870.2010.00478.x

Sangelantoni L, Russo A, Gennaretti F (2018) Impact of bias correction and downscaling through quantile mapping on simulated climate change signal: a case study over Central Italy. Theor Appl Climatol. https://doi.org/10.1007/s00704-018-2406-8

Scoccimarro E, Gualdi S, Bellucci A, Zampieri M, Navarra A (2013) Heavy precipitation events in a warmer climate: results from CMIP5 models. J Clim 26:7902–7911. https://doi.org/10.1175/JCLI-D-12-00850.1

Scoccimarro E, Gualdi S, Navarra A (2016) Heavy precipitation events over the Euro-Mediterranean region in a warmer climate: results from CMIP5 models. Reg Environ Change. https://doi.org/10.1007/s10113-014-0712-y

Segoni S, Piciullo L, Gariano SL (2018) A review of the recent literature on rainfall thresholds for landslide occurrence. Landslides. https://doi.org/10.1007/s10346-018-0966-4

Seneviratne SI, Nicholls N, Easterling D, Goodess CM, Kanae S, Kossin J, Luo Y, Marengo J, McInnes K, Rahimi M, Reichstein M, Sorteberg A, Vera C, Zhang X (2012) Changes in climate extremes and their impacts on the natural physical environment. In: Field CB, Barros V, Stocker TF et al (eds) Managing the risks of extreme events and disasters to advance climate change adaptation. A special report of working groups I and II of the intergovernmental panel on climate change (IPCC). Cambridge University Press, Cambridge, pp 109–230

Sengupta A, Gupta S, Anbarasu K (2010) Rainfall thresholds for the initiation of landslide at Lanta Khola in north Sikkim, India. Nat Hazards 52:31–42. https://doi.org/10.1007/s11069-009-9352-9

Smith PC, Heinrich G, Suklitsch M, Gobiet A, Stoffel M, Fuhreret J (2014) Station-scale bias correction and uncertainty analysis for the estimation of irrigation water requirements in the Swiss Rhone catchment under climate change. Clim Change 127:521–534. https://doi.org/10.1007/s10584-014-1263-4

Switanek MB, Troch PA, Castro CL, Leuprecht A, Chang HI, Mukherjee R, Demaria EMC (2017) Scaled distribution mapping: a bias correction method that preserves raw climate model projected changes. Hydrol Earth Syst Sci 21:2649–2666

Themeßl MJ, Gobiet A, Heinrich G (2011a) Empirical-statistical downscaling and error correction of regional climate models and its impact on the climate change signal. Clim Change 112:449–468. https://doi.org/10.1007/s10584-011-0224-4

Themeßl MJ, Gobiet A, Leuprecht A (2011b) Empirical-statistical downscaling and error correction of daily precipitation from regional climate models. Int J Climatol 1544:1530–1544. https://doi.org/10.1002/joc.2168

Tomozeiu R, Agrillo G, Cacciamani C, Pavan V (2013) Statistically downscaled climate change projections of surface temperature over Northern Italy for the periods 2021–2050 and 2070–2099. Nat Hazards. https://doi.org/10.1007/s11069-013-0552-y

Trenberth KE (1999) Conceptual framework for changes of extreme of the hydrological cycle with climate change.pdf. Clim Change 42:327–339

Turkington T, Remaître A, Ettema J, Hussin H, van Westen C (2016) Assessing debris flow activity in a changing climate. Clim Change 137:293–305. https://doi.org/10.1007/s10584-016-1657-6

Van Meijgaard E, Van Ulft LH, Lenderink G, de Roode SR, Wipfler L, Boers R, Timmermans RMA (2012) Refinement and application of a regional atmospheric model for climate scenario calculations of Western Europe. Climate changes Spatial Planning publication, pp 44

Vennari C, Gariano SL, Antronico L, Brunetti MT, Iovine G, Peruccacci S, Terranova O, Guzzetti F (2014) Rainfall thresholds for shallow landslide occurrence in Calabria, Southern Italy. Nat Hazards Earth Syst Sci 14:317–330. https://doi.org/10.5194/nhess-14-317-2014

Volosciuk C, Maraun D, Semenov VA, Tilinina N, Gulev SK, Latifet M (2016) Rising Mediterranean Sea Surface Temperatures Amplify Extreme Summer Precipitation in Central Europe

Walsh K, Giorgi F, Coppola E (2014) Mediterranean warm-core cyclones in a warmer world. Clim Dyn 42:1053–1066. https://doi.org/10.1007/s00382-013-1723-y

White ID, Mottershead DN, Harrison JJ (1996) Environmental systems, 2nd edn. Chapman & Hall, London, p 616

Wilcke RAI, Mendlik T, Gobiet A (2013) Multi-variable error correction of regional climate models. Clim Change 120:871–887. https://doi.org/10.1007/s10584-013-0845-x

Wilks DS (2006) Statistical methods in the atmospheric sciences, 2nd edn. Elsevier, New York City

WMO, No. 100 (2007) Guide to climatological practices, 3rd edn. WMO, Geneva

Xoplaki E, González-Rouco JF, Luterbacher J, Wanner H (2004) Wet season Mediterranean precipitation variability: influence of large-scale dynamics and trends. Clim Dyn 23:63–78. https://doi.org/10.1007/s00382-004-0422-0

Zappa G, Hawcroft MK, Shaffrey L, Balck E, Brayshaw DJ (2014) Extratropical cyclones and the projected decline of winter Mediterranean precipitation in the CMIP5 models. Clim Dyn. https://doi.org/10.1007/s00382-014-2426-8

Zollo AL, Rianna G, Mercogliano P, Tommasi P, Comegna L (2014) Validation of a simulation chain to assess climate change impact on precipitation induced landslides. In: Sassa K, Canuti K, Yin P (eds) Landslide Science for a Safer Geoenvironment, vol 1. Springer, pp 287–292